

18 August 2020

- **Further work has been conducted on refining the consolidation of drill hole data for the Nxuu Deposit**
- **Paper on Mineralogy and Genesis of Kihabe Zn-Pb-V Deposit conducted by Naples University published – MDPI Minerals Journal.**

CONSOLIDATION OF NXUU DEPOSIT DRILL HOLE DATA

Further to the announcement released to the market on 6 August 2020, the Company has spent further time in refining the presentation of data for holes drilled into the Nxuu Deposit to date.

The drill hole map for Nxuu Deposit North (Figure 1) now highlights a South West Area (see Figure 2) and a Remaining Area (see Figure 3).

Figure 2, Nxuu Deposit North, South West Area shows just the mineralised domains of NXDD037, NXRC027, NXDD003 and NXDD036. Figure 2(a) shows the assay grades of the mineralised domains of those same holes.

Figure 3, Nxuu Deposit North Remaining Area Drill Hole Map shows just the mineralised domains of the other 20 holes drilled into the Nxuu Deposit. For the sake of continuity NXRC036 shown in Figure 2 is also shown in Figure 3. Figures 3 (a) to 3 (j) show assay grades of the mineralised domains of the same drill holes.

By presenting the data in this manner the Company believes Figure 2 and Figure 3 show more clearly the continuity of the mineralised domain of the Nxuu Deposit as known from holes drilled to date. Figure 2 (a) and FigureS 3(a) to 3 (j) show the assay grades of those drill holes more clearly, compared with compacting all the assay data on Figures 2 and 3.

Nxuu Deposit is a basin-shaped deposit where mineralisation in a totally oxidised quartz wacke extends to a maximum depth of 60m. Extractive metallurgical test work on samples of Nxuu Zn/Pb mineralisation shows that 93% Zn can be recovered in 12 hours via acid leach, with the potential to produce Zn metal on site through SX/EW, with 93% Pb reporting to flotation concentrate.

More recently it has been demonstrated on a similar deposit in Australia that lead carbonate can be successfully extracted using methane sulphonic acid followed by SX/EW, allowing for Pb to also be recovered on site. This test work has yet to be conducted on the Nxuu Deposit.

Recent metallurgical test work on Nxuu mineralisation has shown that 80.4% Vanadium Pentoxide (V₂O₅) can be recovered on site through a standard oxide flotation process using a hydroxamate collector for recovery.

Previous Nxuu resource estimates, reported under the 2004 JORC Code only included Zn/Pb. Since production of those estimates, a significant amount of additional drilling has been conducted and it is now evident that V₂O₅ will represent a substantial additional credit. Accordingly, the old 2004 JORC resource estimates do not reflect the actual mineralisation encountered at Nxuu. On completion of a further 2,500m of drilling, the Company will be able to quote a resource compliant with the 2012 JORC Code.

The Company plans to develop the Nxuu Deposit first as it is seen as a potentially shallow, low risk and low cost operation.

Potential Contribution of Vanadium Pentoxide and Germanium

Based on historical results of previous explorers, the Company's initial premise when it first acquired the Kihabe Project in 2003 was that Kihabe and Nxuu contained only Zn/Pb mineralisation. Consequently, holes in the Company's earlier drilling campaigns were not always assayed for Vanadium/Vanadium Pentoxide (V/V₂O₅) and/or Germanium (Ge).

Vanadium/Vanadium Pentoxide

Review of results from recent drilling campaigns that included assaying for Vanadium, show that this mineralisation at the Nxuu Deposit extends beyond the zones of Zn/Pb mineralisation, thereby increasing the overall metal endowed domains within the mineralised quartz wacke.

As previously reported:

- Mineralogical test work has confirmed that V/V₂O₅ in the Nxuu Deposit is hosted in the oxide vanadate DESCLOIZITE, where V₂O₅ is 1.785 times the volume of V. (Refer to revised announcement released by the Company on 12 December 2018)
- Metallurgical test work has shown that V₂O₅ can be extracted on site through the process of flotation using a hydroxamate collector for recovery (Refer to announcement released by the Company on 10 January 2019). Accordingly, V₂O₅ could represent a significant credit for the Project.

Average Volume of Recoverable Mineralisation

Of the 24 holes drilled to date into the whole of the Nxuu Deposit, close to 58%, on average, of every hole contains recoverable Zn/Pb/V₂O₅ mineralisation. Of the remaining 42%, 17% consists of Kalahari sand cover, leaving only 25% as insignificantly mineralised quartz wacke.

Average Depth to Base of Mineralisation

The average depth to the base of Zn/Pb/V₂O₅ mineralisation of the 24 holes so far drilled into the Nxuu Deposit is just under 40m, which confirms its shallow nature.

Germanium

Nxuu Deposit samples containing Germanium have been sent to the University of Naples for test work to determine the nature and structure of the host mineral. Once out of lockdown, Naples University will be able to commence this test work. If shown to be recoverable, this could also represent a further credit for the Project as Ge is currently trading at US \$1,890/kg. In 1992, in order to prove extraction of Gallium and Germanium from domestic sources, the USBM demonstrated that both these semi-metals could be extracted into solution by sulphuric acid leach with further downstream recovery. As can be seen in Nxuu drill holes containing germanium, it occurs within the zones containing Zn/Pb/Ag/V₂O₅, so it would be extracted as part of normal mining operations.

Further Ge samples have recently been sent to Roger Townend, mineralogist. These samples have now been sent to CSIRO for mineralogical test work in an effort to identify the host oxide mineral of Ge.

NXUU DEPOSIT RECOVERABLE VANADIUM PENTOXIDE (V₂O₅) GRADE

As reported on 22 January 2019, recoverable V₂O₅ grades were calculated as follows:

- Through applying the factor of 1.785 to all previous Vanadium metal assay grades reported under both the 2004 and 2012 JORC Codes, the Company has re-calculated the VANADIUM PENTOXIDE (V₂O₅) grades as shown on the Figures 2 and 3.
- Based on metallurgical test work recovery results, confirmed by ALS Laboratories, the Company has discounted the V₂O₅ grades to 80% to show the **RECOVERABLE** grades as shown **(in brackets)** in Figures 2 (a) and 3 (a) to 3 (j).

The Vanadium mineral DESCLOIZITE can be treated on site to produce V₂O₅ which can then be sold as a marketable product.

NXUU DEPOSIT RECOVERABLE ZINC EQUIVALENT GRADE APPLYING A 1% ZINC EQUIVALENT LOW CUT

As reported on 22 January 2019 the Zn equivalent grades were calculated as follows:

The Zinc Equivalent Grade for the Nxuu Deposit includes grades of Zinc, Lead and Silver, calculated by applying the average of five trading days LME closing prices for Zinc and Lead and the five trading days of USA closing prices for Silver, from 22 to 26 January 2018. Zinc and Lead grade values were then discounted to 93% to reflect the **RECOVERABLE** value based on metallurgical test work conducted by AMMTEC. Silver grade values were then discounted to 70% to reflect **RECOVERABLE** value of Silver as achieved in similar deposits.

- LME average closing Zinc price of US\$ 3,464/t, being US\$ 34.64 per 1% was reduced to **US\$32.21 per 1%** to reflect a recovery of 93% as demonstrated in previous metallurgical test work conducted by AMMTEC.
- LME average closing Lead price of US\$ 2,611/t, being US\$ 26.11 per 1% was reduced to **US\$24.28 per 1%** to reflect a recovery of 93% as demonstrated in previous metallurgical test work conducted by AMMTEC.
- USA average Day Trade closing Silver price of US\$ 17.23/oz, being US\$ 0.55/g reduced to **US\$0.38/g** to reflect a recovery of 70% based on recovery performance of similar deposits. (Refer to Estimated Silver Recovery below)

Combined total discounted US\$ value of each assay including any or all of Zinc, Lead and Silver was then divided by the discounted calculated Zinc price of US\$32.21 per 1% to arrive at the **RECOVERABLE** Zinc Equivalent Grade. Only resulting grades of over 1% Zinc Equivalent were then applied in determining widths of mineralised intersections reported to ASX.

To evaluate current zinc equivalent grades the Zn/Pb/Ag prices of January 2018 are compared with current day prices (14 August 2020) to reflect any impact on the Zn equivalent grades applied.

January 2018 prices	US\$	%	Current Prices	US\$	%
Zinc	3,464	57	Zinc	2,360	55
Lead	2,611	43	Lead	1,946	45
	6,075	100		4,306	100
Silver	17.23		Silver	26.72	

The Zn equivalent grade is calculated on percentage contribution relative to the grade and value of each metal. As there is little difference between relative value of these metals, the Company believes there is no need to recalculate the Zn equivalent grade for the current value despite the significant variance in current metal prices compared with those of January 2018. The Zn/Pb grades are the same as those used in January 2018. There is only a 2% variance in the contribution each metal makes according to their current prices.

Zinc Equivalent Recoverable Grade -Calculation Formula

- US\$ Zinc price/t divided by 100 = US \$ Zinc price per 1% X 93% Recovery X Zinc Grade % = US\$A
- US\$ Lead price/t divided by 100 = US \$ Lead price per 1% X 93% Recovery X Lead Grade % = US\$B
- US\$ Silver price/oz divided by 31.1 = US \$ Silver price per gram X 70% Recovery X Silver Grade g/t = US\$C

$$\text{US\$A} + \text{US\$B} + \text{US\$ C} \text{ divided by US\$A} = \text{Zinc Equivalent Grade}$$

INVESTIGATION INTO THE MINERALOGY AND GENESIS OF THE KIHABE Zn-Pb-V DEPOSIT

The Company has recently received a copy of a publication, published in the journal Minerals. This publication consisted of work conducted by Maria Boni, Dr Mondillo, Giuseppina Balassone, Francesco Putzolu and Licia Santoro of Naples University on the mineralogy and genesis of the Kihabe Deposit.

Samples from holes drilled into the Kihabe Deposit were sent by the Company to Naples University for this investigative work to be conducted.

A copy of the publication is attached.

Forward Looking Statement

This report contains forward looking statements in respect of the projects being reported on by the Company. Forward looking statements are based on beliefs, opinions, assessments and estimates based on facts and information available to management and/or professional consultants at the time they are formed or made and are, in the opinion of management and/or consultants, applied as reasonably and responsibly as possible as at the time that they are applied.

Any statements in respect of Ore Reserves, Mineral Resources and zones of mineralisation may also be deemed to be forward looking statements in that they contain estimates that the Company believes have been based on reasonable assumptions with respect to the mineralisation that has been found thus far. Exploration targets are conceptual in nature and are formed from projection of the known resource dimensions along strike. The quantity and grade of an exploration target is insufficient to define a Mineral Resource. Forward looking statements are not statements of historical fact, they are based on reasonable projections and calculations, the ultimate results or

outcomes of which may differ materially from those described or incorporated in the forward looking statements. Such differences or changes in circumstances to those described or incorporated in the forward looking statements may arise as a consequence of the variety of risks, uncertainties and other factors relative to the exploration and mining industry and the particular properties in which the Company has an interest.

Such risks, uncertainties and other factors could include but would not necessarily be limited to fluctuations in metals and minerals prices, fluctuations in rates of exchange, changes in government policy and political instability in the countries in which the Company operates.

Other important Information

Purpose of document: This document has been prepared by Mount Burgess Mining NL (MTB). It is intended only for the purpose of providing information on MTB, its project and its proposed operations. This document is neither of an investment advice, a prospectus nor a product disclosure statement. It does not represent an investment disclosure document. It does not purport to contain all the information that a prospective investor may require to make an evaluated investment decision. MTB does not purport to give financial or investment advice.

Professional advice: Recipients of this document should consider seeking appropriate professional advice in reviewing this document and should review any other information relative to MTB in the event of considering any investment decision.

Forward looking statements: This document contains forward looking statements which should be reviewed and considered as part of the overall disclosure relative to this report.

Disclaimer: Neither MTB nor any of its officers, employees or advisors make any warranty (express or implied) as to the accuracy, reliability and completeness of the information contained in this document. Nothing in this document can be relied upon as a promise, representation or warranty.

Proprietary information: This document and the information contained therein is proprietary to MTB.

Competent Persons' Statements:

The information in this report that relates to drilling results at the Nxuu Deposit fairly represents information and supporting documentation approved for release by Giles Rodney Dale FRMIT who is a Fellow of the Australasian Institute of Mining & Metallurgy. Mr Dale is engaged as an independent Geological Consultant to the Company. Mr Dale has sufficient experience which is relevant to the style of mineralisation and type of deposit under consideration and to the activity which he is undertaking to qualify as a Competent Person as defined in the 2012 Edition of the 'Australasian Code for Reporting of Mineral Resources and Ore Reserves (the JORC Code)'. Mr Dale consents to the inclusion in this report of the drilling results and the supporting information in the form and context as it appears.

The information in this report that relates to mineralogical and metallurgical test work results conducted on samples from the Nxuu Deposit fairly represents information and supporting documentation approved for release by Mr Chris Campbell-Hicks, Metallurgist, FAusIMM (CP Metallurgy), MMICA, Non-Executive Director of the Company, who reviewed the content of the announcement. Mr Campbell-Hicks has sufficient experience that is relevant to the style of mineralisation and type of deposit under consideration and to the activity being undertaken to qualify as a Competent Person as defined in the 2012 Edition of the JORC Code and has consented to the inclusion in respect of the matters based on the information in the form and context in which it appears.

Mr Campbell-Hicks has for a number of years whilst working with Coffey Mining and other consultancies and companies made contributions to numerous Scoping Studies, Pre-feasibility Studies and Feasibility Studies under the 2004 JORC Code, the 2012 JORC Code and the Canadian National Instrument (NI 43-101). As such he qualifies as a Competent Person for reporting on matters pertaining to metallurgy, process engineering and interpretation of test work results and data for the establishment of Design Criteria for such studies.

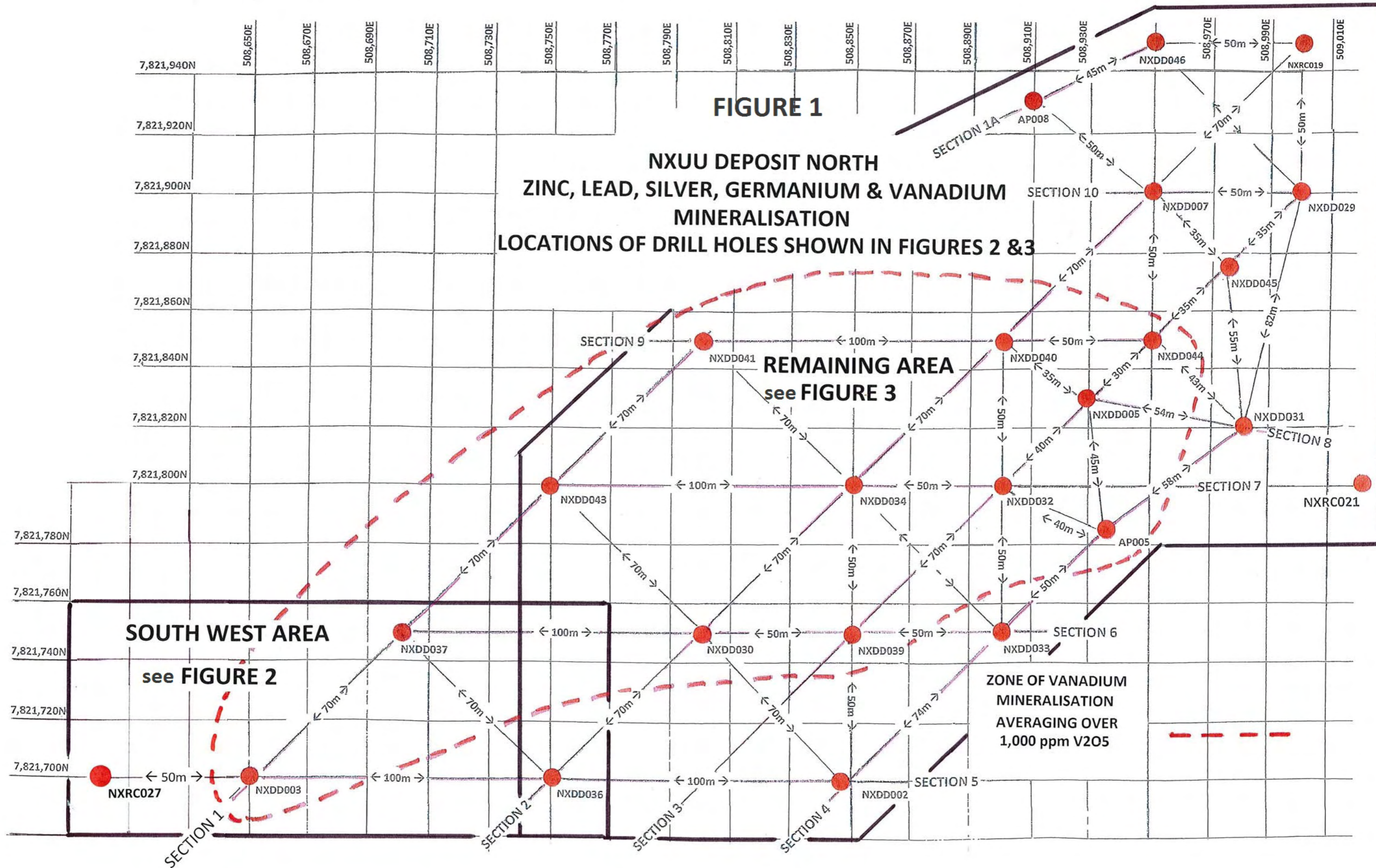


FIGURE 1

**NXUU DEPOSIT NORTH
ZINC, LEAD, SILVER, GERMANIUM & VANADIUM
MINERALISATION
LOCATIONS OF DRILL HOLES SHOWN IN FIGURES 2 & 3**

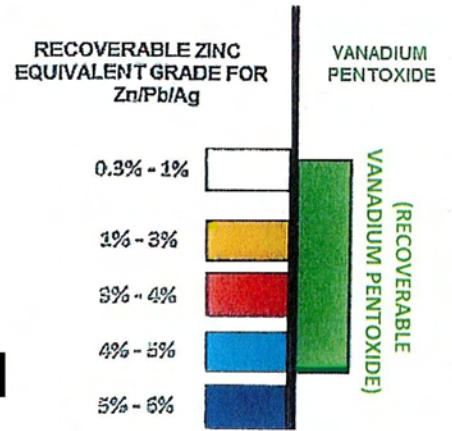
**REMAINING AREA
see FIGURE 3**

**SOUTH WEST AREA
see FIGURE 2**

**ZONE OF VANADIUM
MINERALISATION
AVERAGING OVER
1,000 ppm V2O5**

NXUU DEPOSIT NORTH SOUTH WEST AREA DRILL HOLE SECTIONS

LEGEND



GERMANIUM

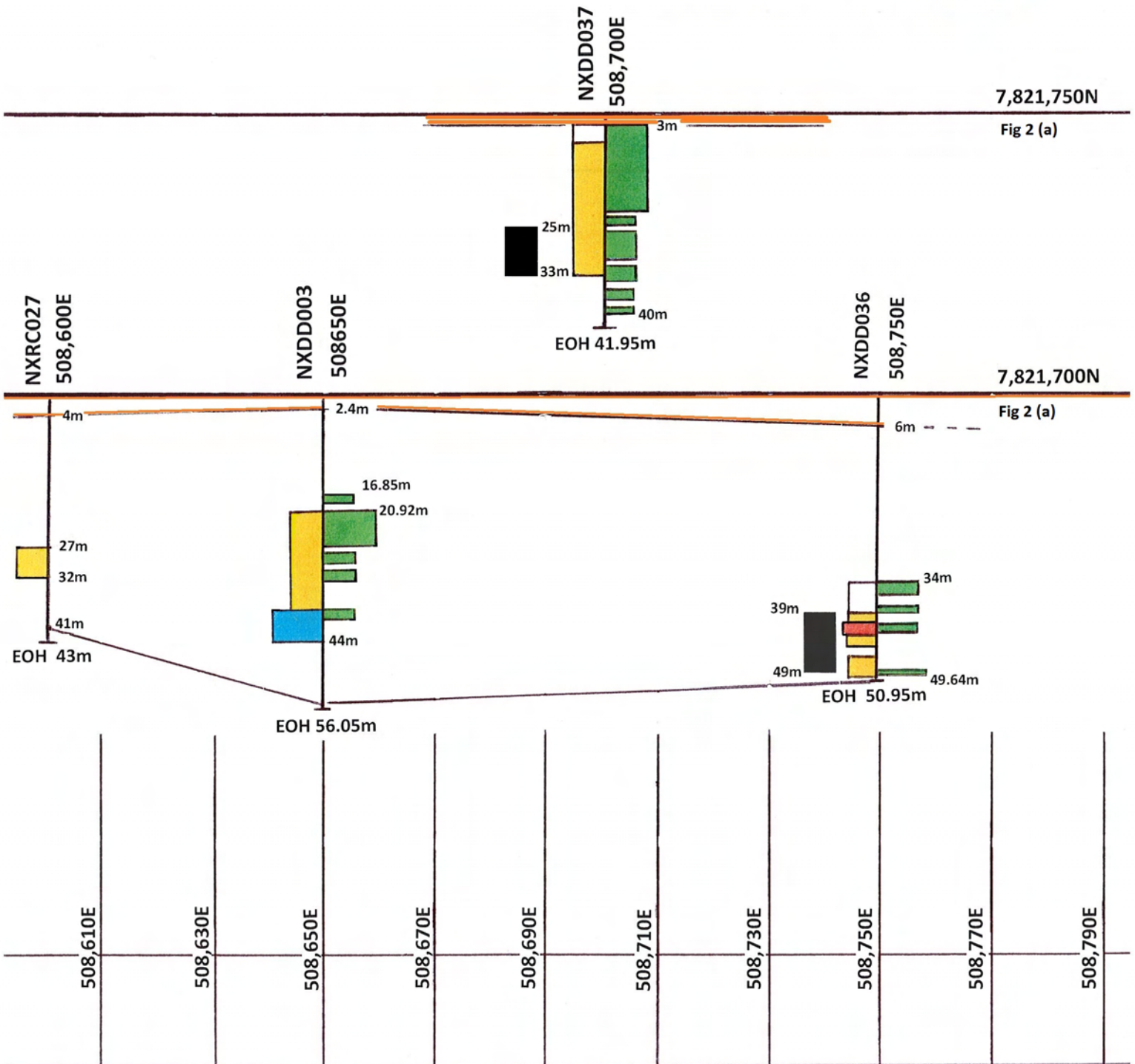
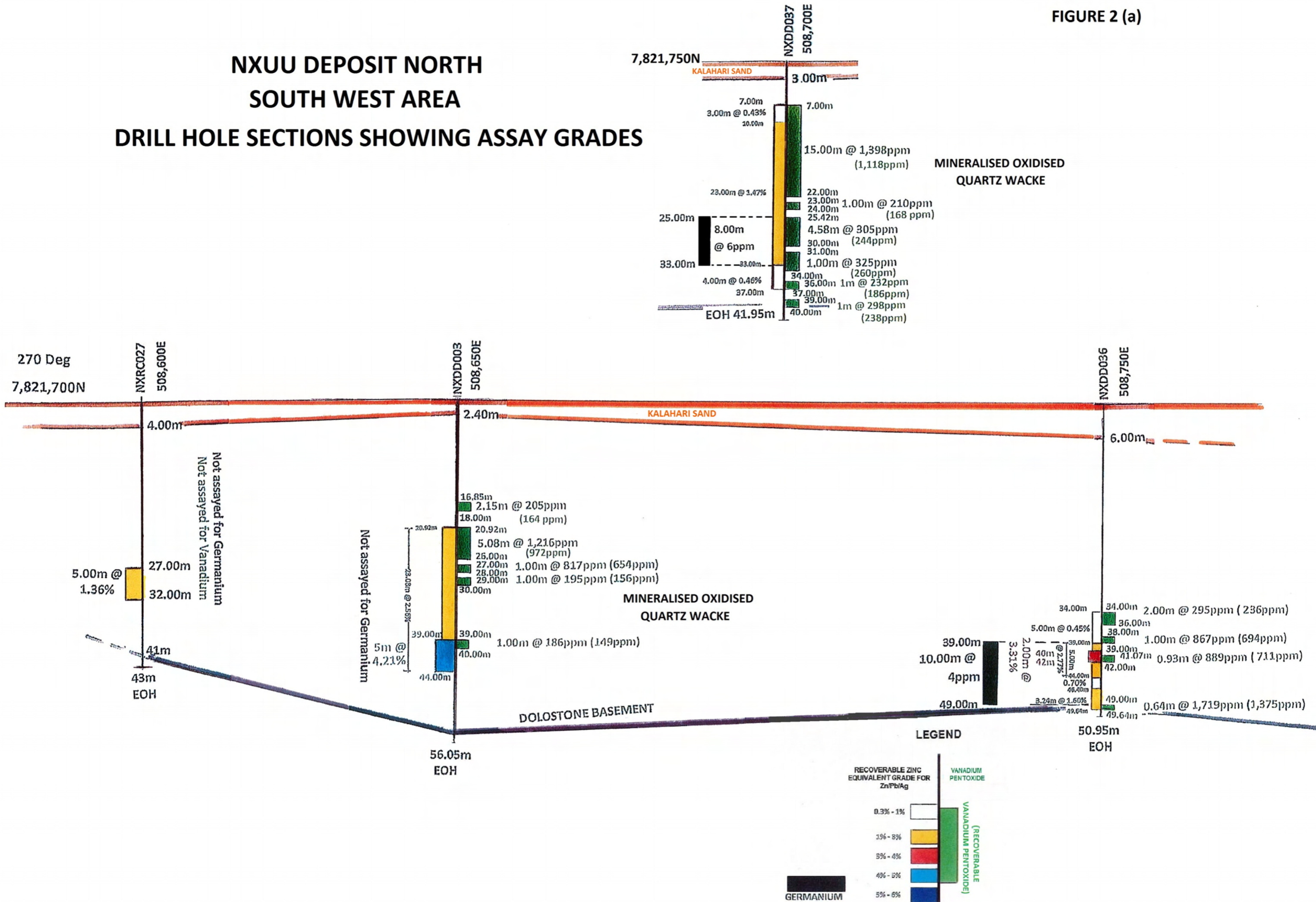


FIGURE 2 (a)

NXUU DEPOSIT NORTH SOUTH WEST AREA DRILL HOLE SECTIONS SHOWING ASSAY GRADES



NXUU DEPOSIT NORTH REMAINING AREA DRILL HOLE MAP

FIGURE 3

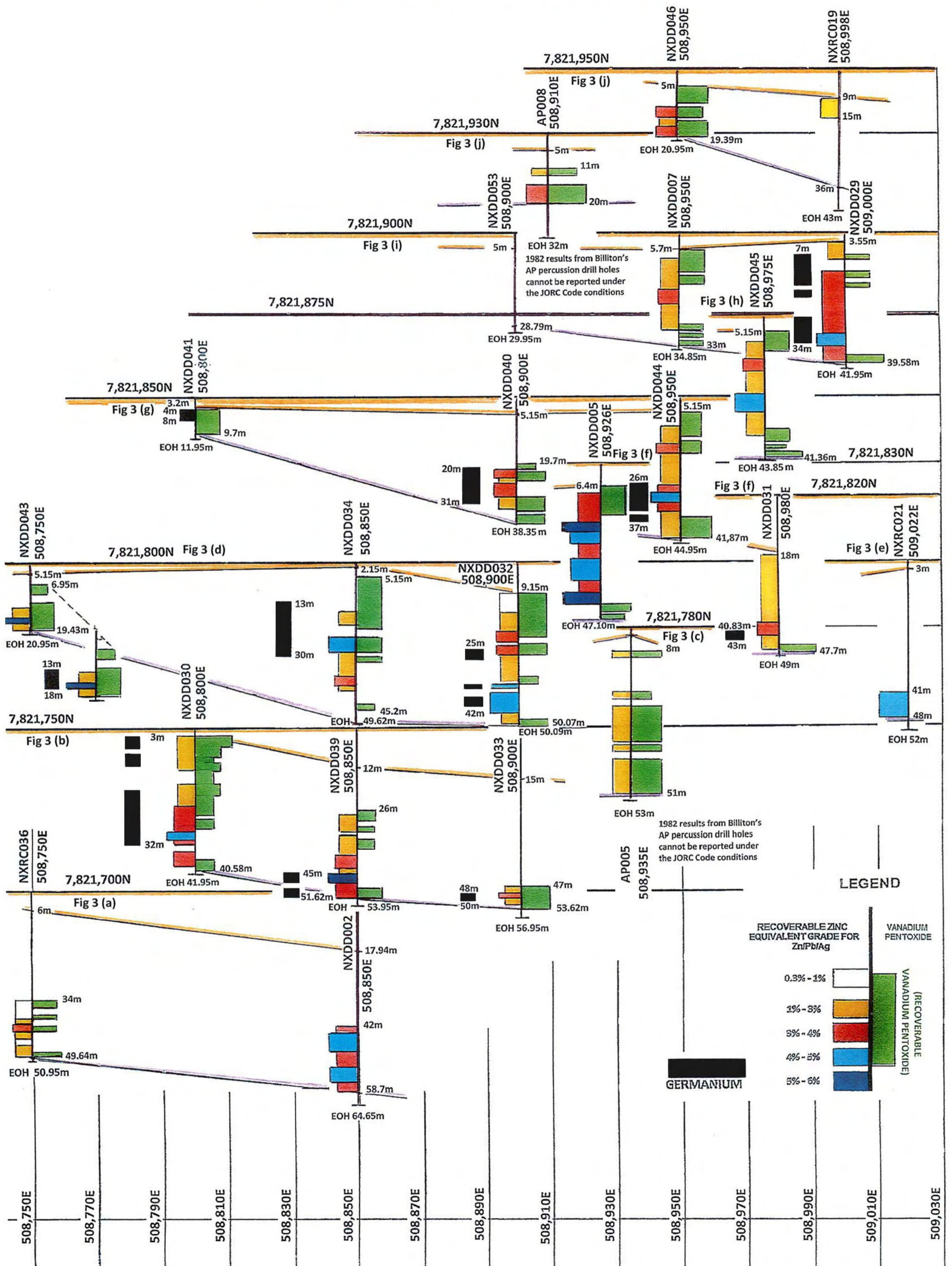


FIGURE 3 (a)

NXUU DEPOSIT NORTH

DRILL HOLE SECTIONS SHOWING ASSAY GRADES



LEGEND

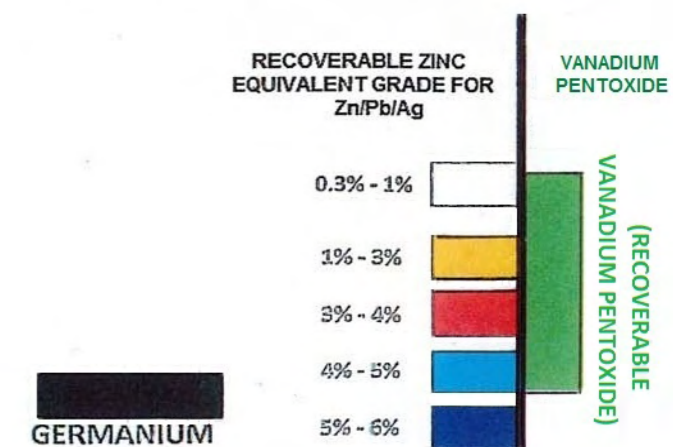
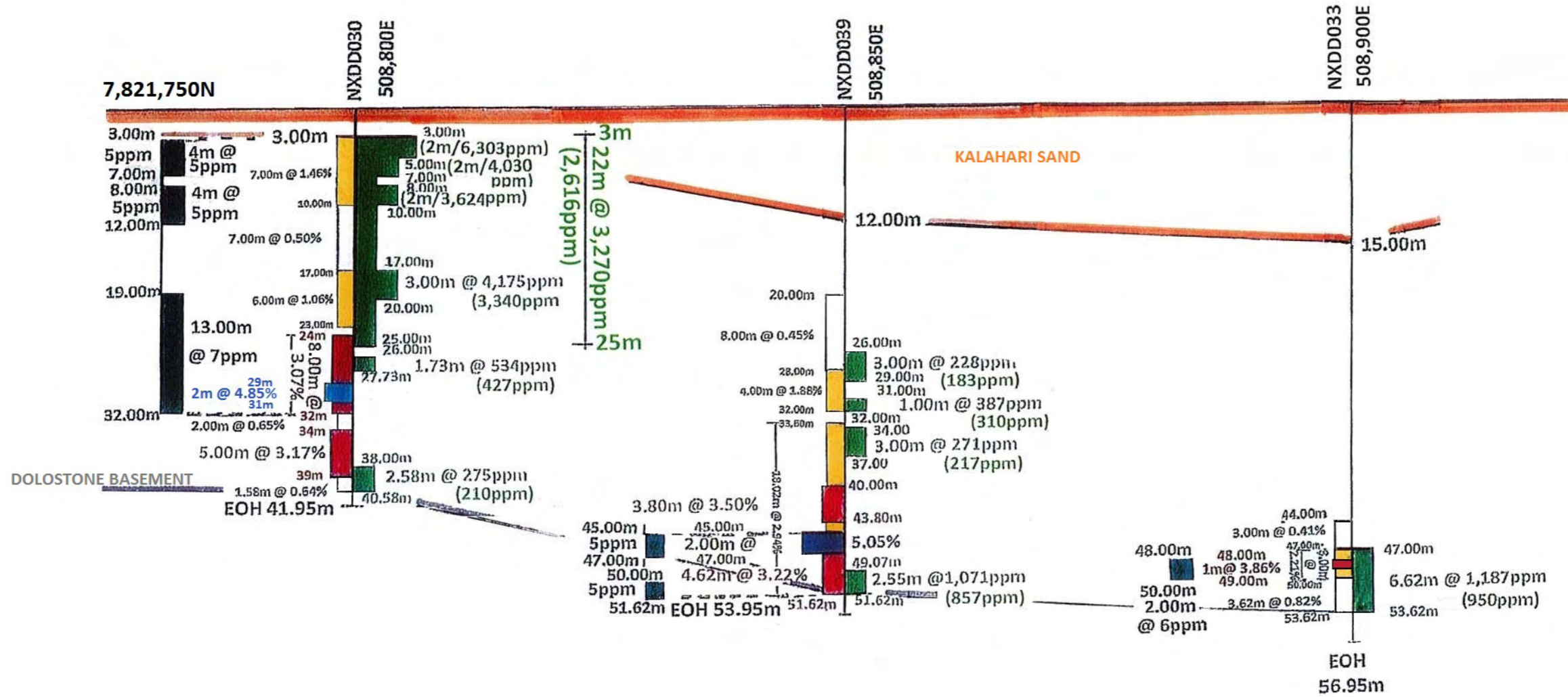
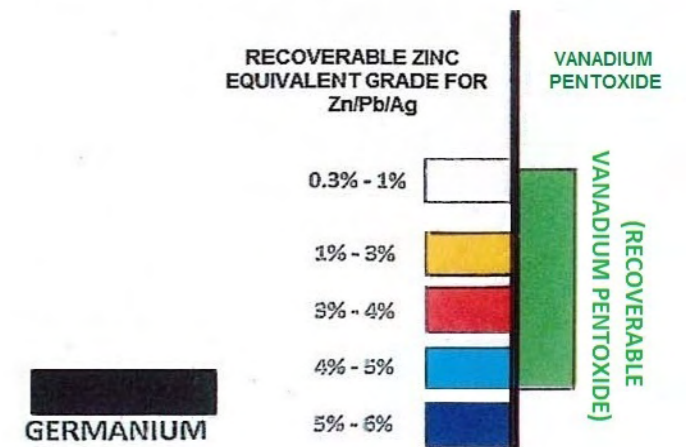


FIGURE 3 (b)

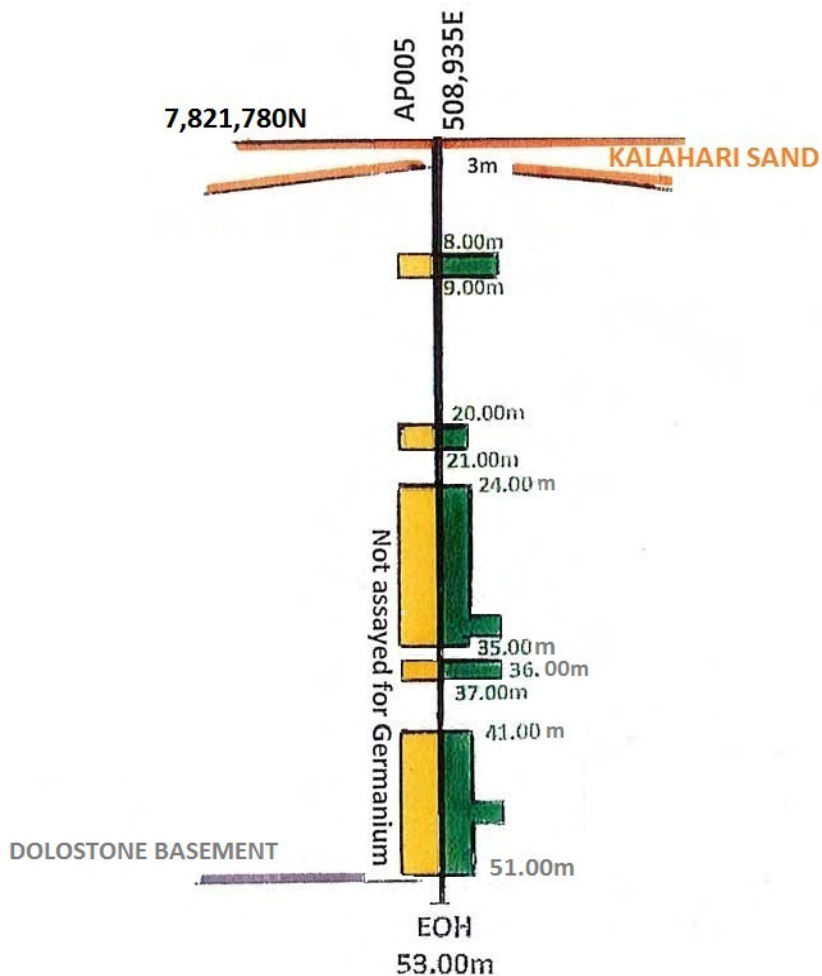
NXUU DEPOSIT NORTH DRILL HOLE SECTIONS SHOWING ASSAY GRADES



LEGEND

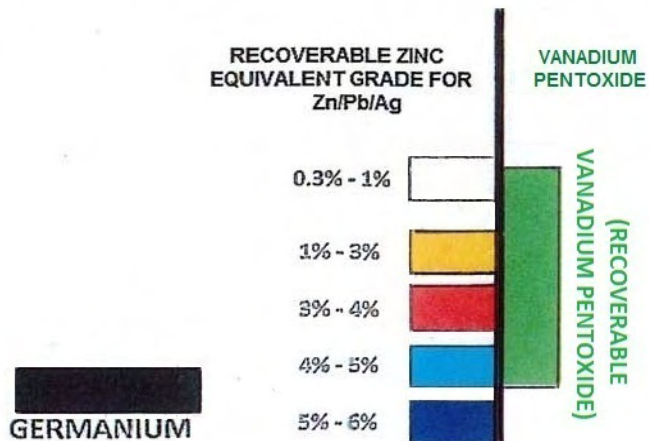


NXUU DEPOSIT NORTH
 DRILL HOLE SECTIONS SHOWING ASSAY GRADES



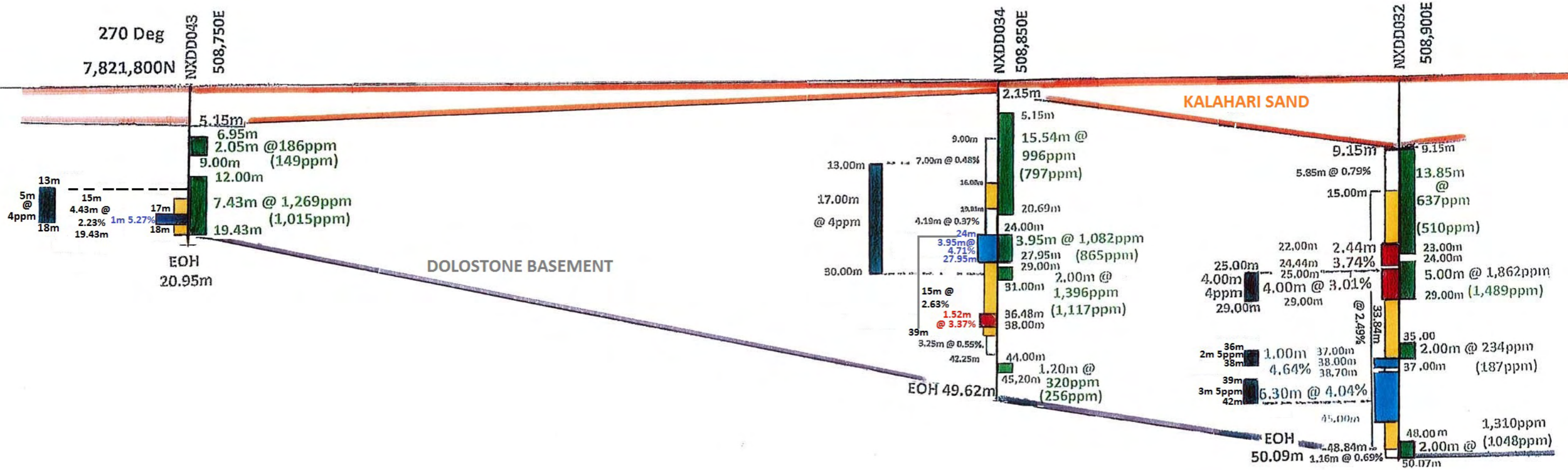
Results from Billiton's 1982 AP percussion drill holes cannot be reported under the JORC Code conditions

LEGEND

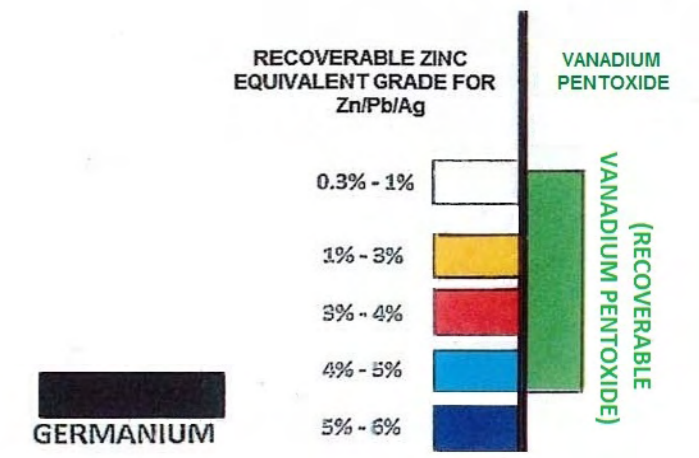


NXUU DEPOSIT NORTH DRILL HOLE SECTIONS SHOWING ASSAY GRADES

FIGURE 3 (d)

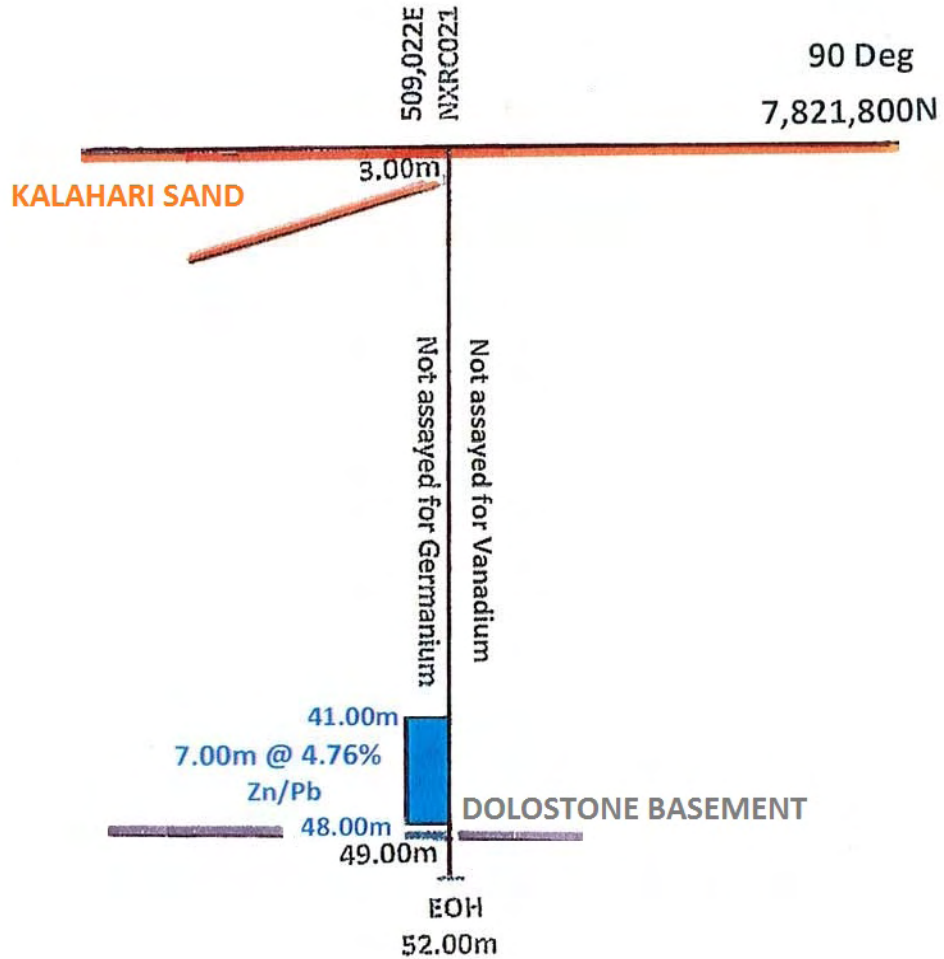


LEGEND

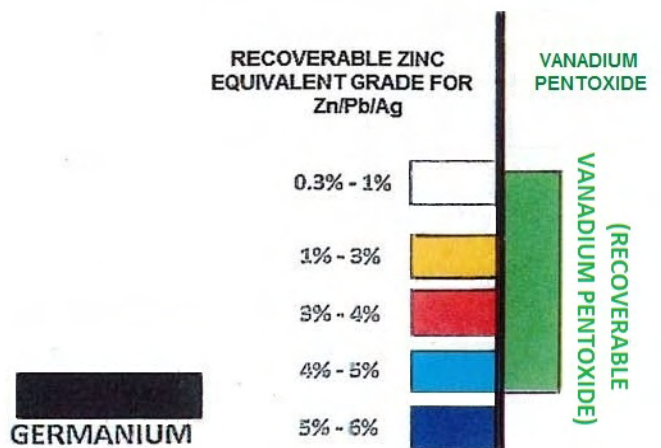


NXUU DEPOSIT NORTH DRILL HOLE SECTIONS SHOWING ASSAY GRADES

FIGURE 3 (e)



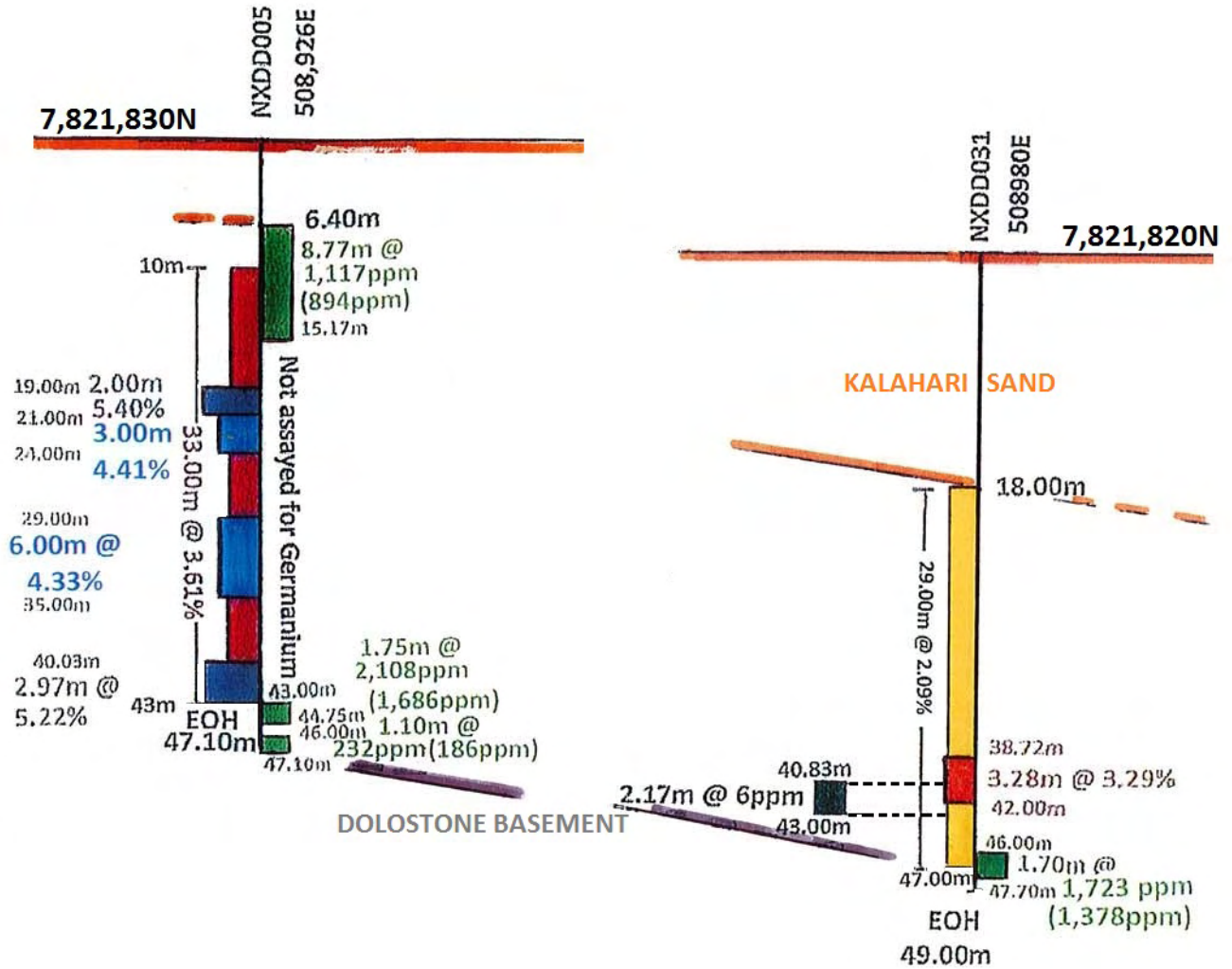
LEGEND



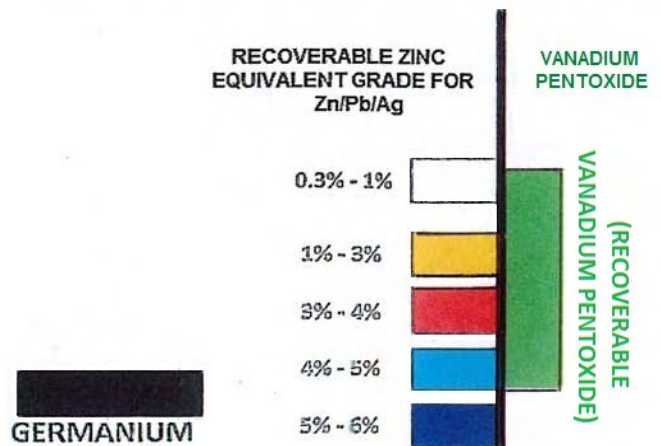
NXUU DEPOSIT NORTH

FIGURE 3 (f)

DRILL HOLE SECTIONS SHOWING ASSAY GRADES



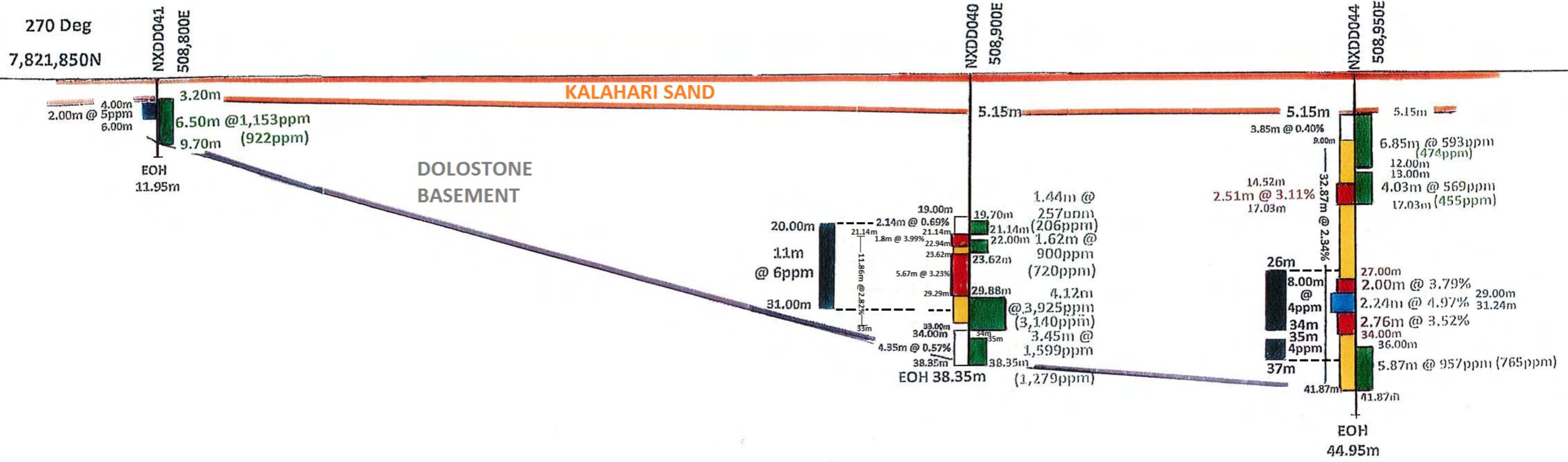
LEGEND



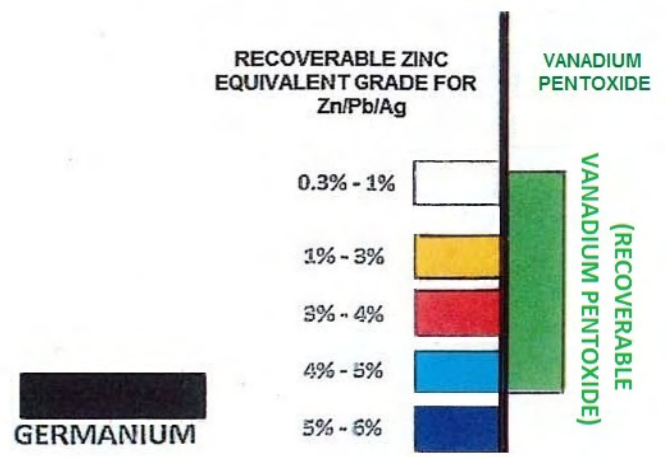
NXUU DEPOSIT NORTH

FIGURE 3 (g)

DRILL HOLE SECTIONS SHOWING ASSAY GRADES

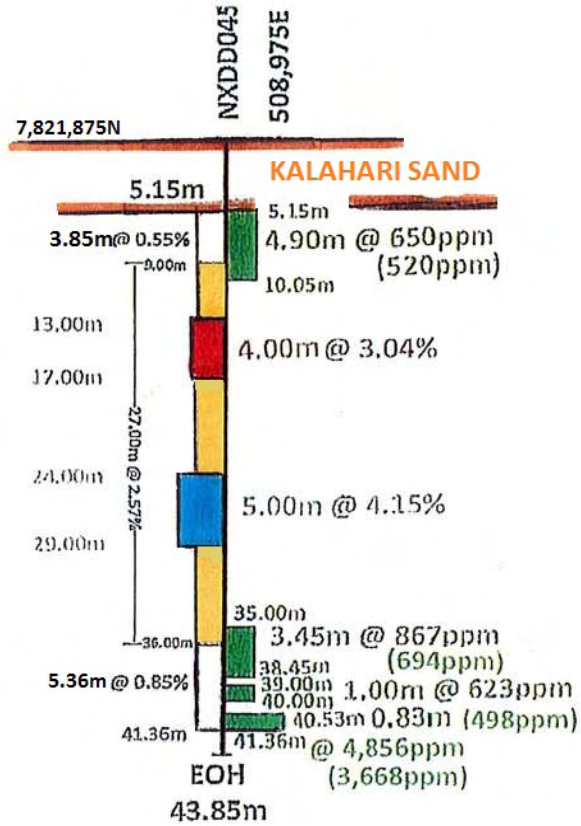


LEGEND

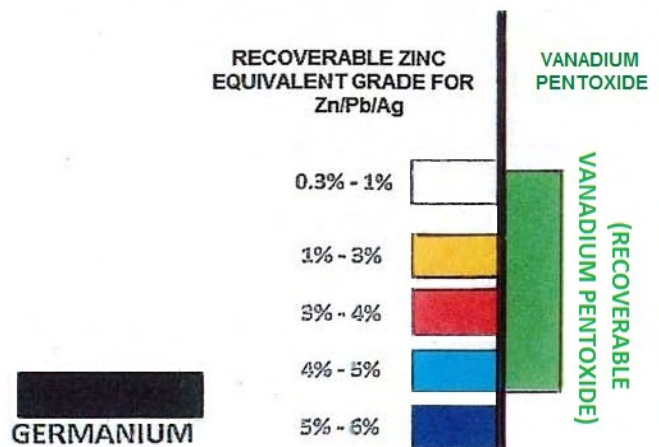


NXUU DEPOSIT NORTH

DRILL HOLE SECTIONS SHOWING ASSAY GRADES

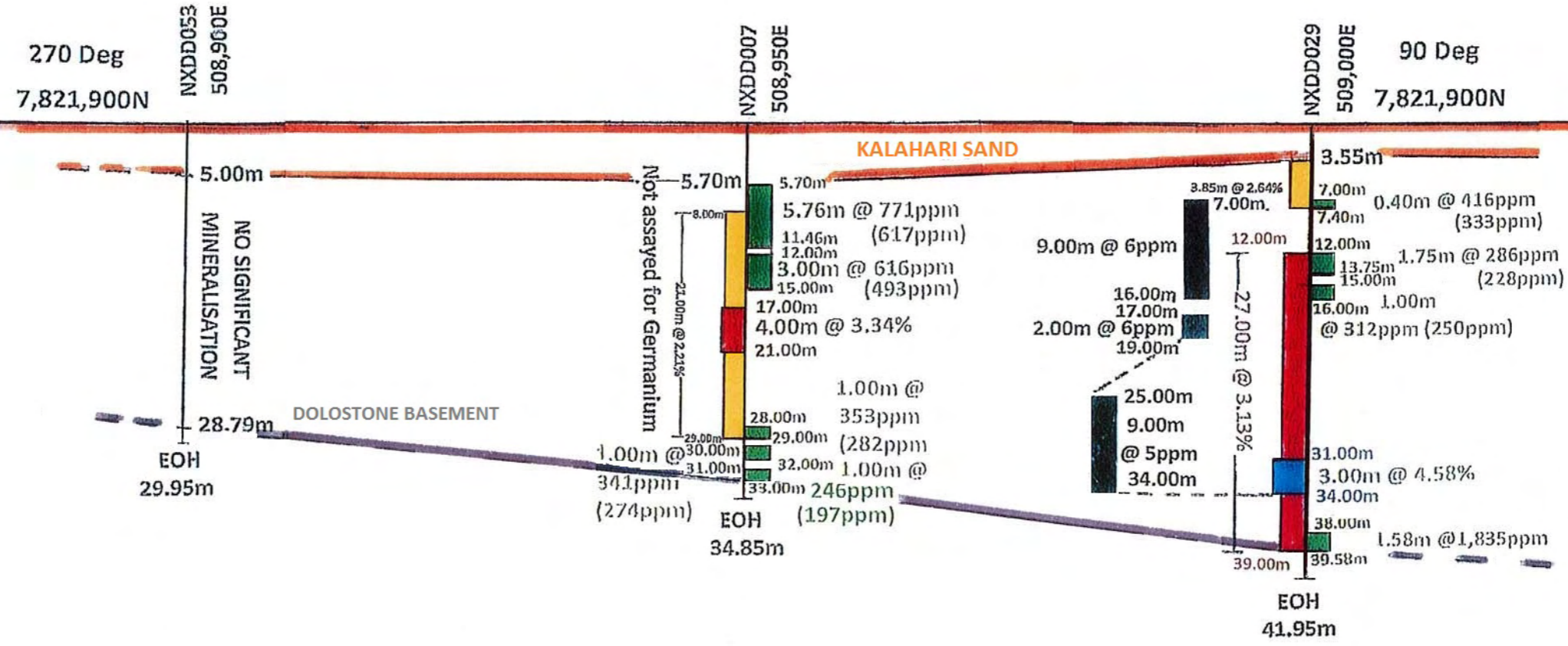


LEGEND



NXUU DEPOSIT NORTH DRILL HOLE SECTIONS SHOWING ASSAY GRADES

FIGURE 3 (i)



LEGEND

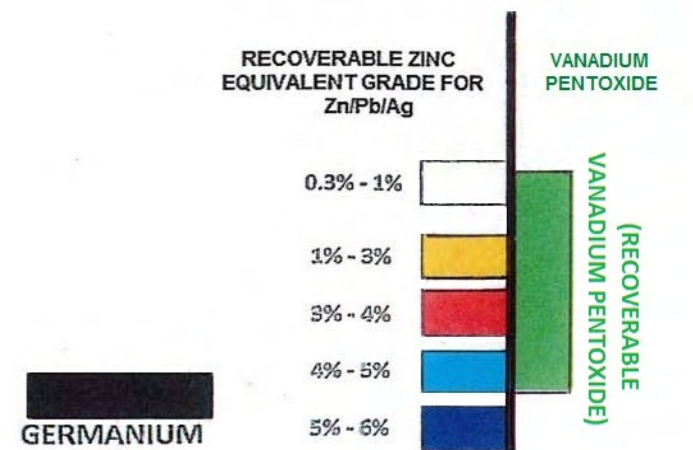
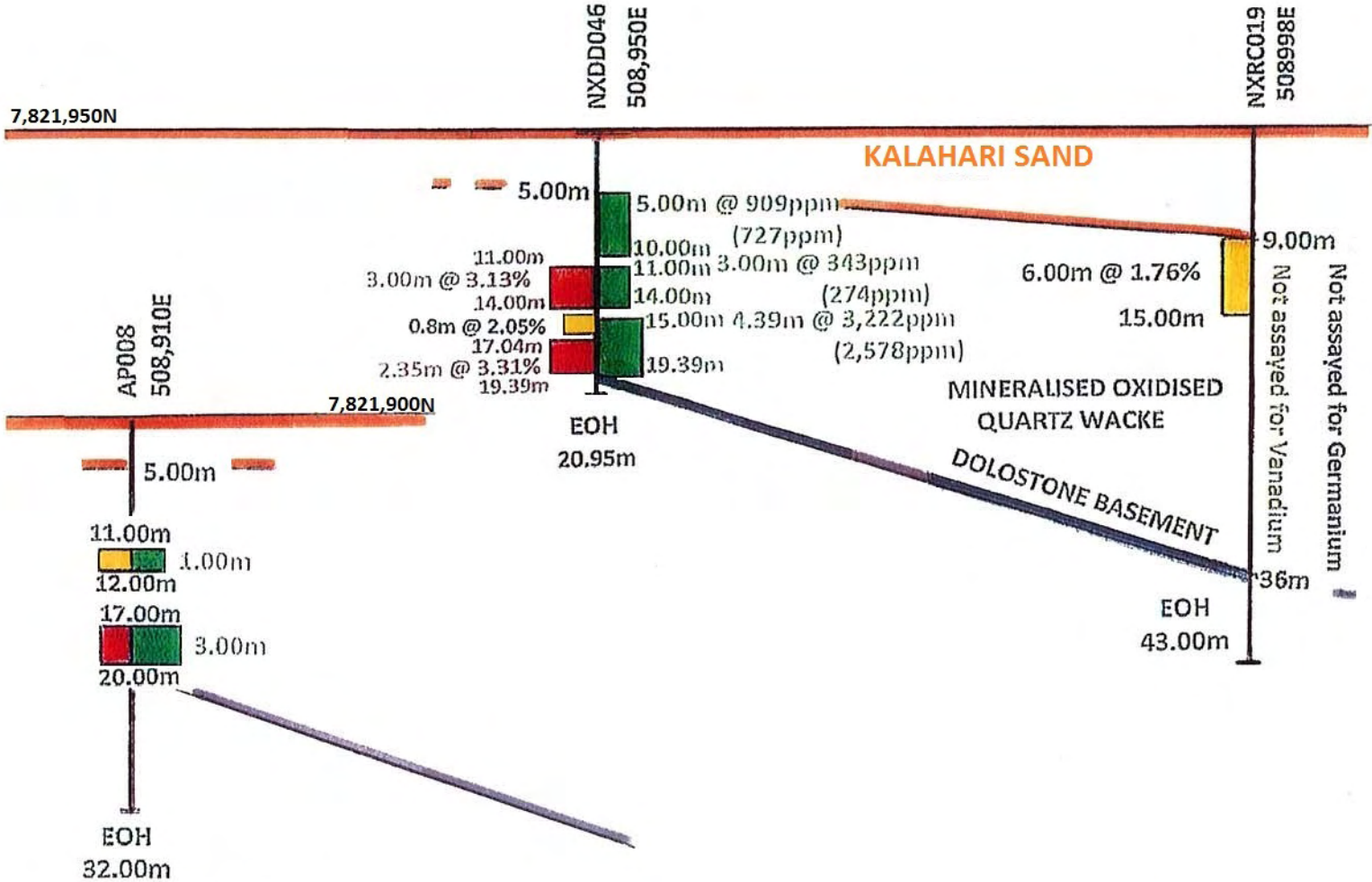


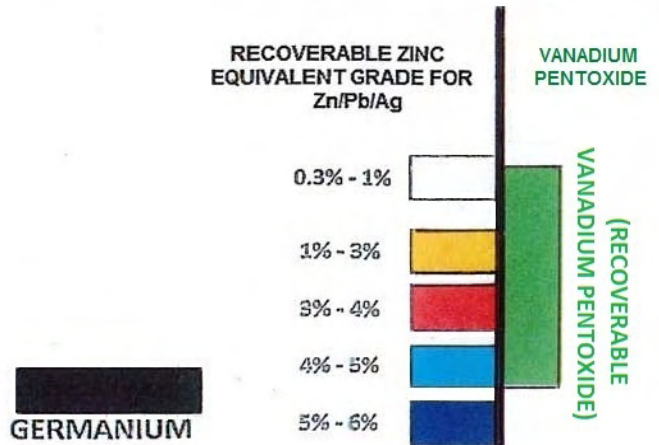
FIGURE 3 (j)

NXUU DEPOSIT NORTH DRILL HOLE SECTIONS SHOWING ASSAY GRADES




Results from Billiton's 1982 AP percussion drill holes cannot be reported under the JORC Code conditions

LEGEND



Article

Mineralogy and Genesis of the Kihabe Zn-Pb-V Prospect, Aha Hills, Northwest Botswana

Nicola Mondillo ^{1,2,*}, Maria Boni ^{1,2}, Giuseppina Balassone ¹, Nigel Forrester ³,
Francesco Putzolu ¹  and Licia Santoro ²

¹ Dipartimento di Scienze della Terra, dell'Ambiente e delle Risorse, Università degli Studi di Napoli Federico II, 80126 Napoli, Italy; boni@unina.it (M.B.); balasson@unina.it (G.B.); francesco.putzolu@unina.it (F.P.)

² Earth Sciences Department, Natural History Museum, Cromwell Road, London SW7 5BD, UK; licia.santoro85@gmail.com

³ Mount Burgess Mining N.L., East Victoria Park 6101, Australia; Nigel@mountburgess.com

* Correspondence: nicola.mondillo@unina.it

Received: 26 June 2020; Accepted: 27 July 2020; Published: 31 July 2020



Abstract: The Kihabe Zn-Pb-V > (Cu-Ag-Ge) prospect is located at the boundary between Namibia and Botswana (Aha Hills, Ngamiland District) in a strongly deformed Proterozoic fold belt, corresponding to the NE extension of the Namibian Damara Orogen. The Kihabe prospect contains Zn-Pb resources of 14.4 million tonnes at 2.84% zinc equivalent, Ag resources of 3.3 million ounces, and notable V-Ge amounts, still not evaluated at a resource level. The ores are represented by a mixed sulfide–nonsulfide mineralization. Sulfide minerals consist mainly of sphalerite, galena and pyrite in a metamorphic quartzwacke. Among the nonsulfide assemblage, two styles of mineralization occur in the investigated samples: A first one, characterized by hydrothermal willemite and baileychlore, and a second one consisting of supergene smithsonite, cerussite, hemimorphite, Pb-phosphates, arsenates and vanadates. Willemite is present in two generations, which postdate sulfide emplacement and may also form at their expenses. These characteristics are similar to those observed in the willemite occurrences of the nearby Otavi Mountainland, which formed through hydrothermal processes, during the final stages of the Damara Orogeny. The formation of the Kihabe willemite is likely coeval. Baileychlore is characterized by textures indicating direct precipitation from solutions and dissolution–crystallization mechanisms. Both processes are typical of hydrothermal systems, thus suggesting a hydrothermal genesis for the Kihabe Zn-chlorite as well. Baileychlore could represent an alteration halo possibly associated either with the sulfide or with willemite mineralization. The other nonsulfide minerals, smithsonite, cerussite, various Pb-phosphates and vanadates, are clearly genetically associated with late phases of supergene alteration, which overprinted both the sulfide and the willemite- and baileychlore-bearing mineralizations. Supergene alteration probably occurred in this part of Botswana from the Late Cretaceous to the Miocene.

Keywords: Botswana; Aha Hills; sulfides; nonsulfides; willemite; baileychlore; chlorite; smithsonite

1. Introduction

Mineral exploration and mining in Botswana has been historically dominated by diamonds and, to lesser extent, by base metals. Copper, gold and nickel have held significant, though smaller, roles in the economy [1]. In particular, after the early 2000s, exploration for Cu-Ag deposits intensified in western parts of Botswana, in the so-called Kalahari Copper Belt (KCB) [1]. Among the various metallogenic regions of the country, the only zone currently showing mineral potential for polymetallic Zn-Pb-Cu-Ag-V-Ge is in northwest Botswana, which represents the northeastern extension of the Namibian Damara Belt [1] (Figures 1 and 2). This is because the Damara Belt of the nearby Otavi

Mountainland (OML) in Namibia is host to several base metal ore deposits [2]. These deposits can be grouped into at least four ore types: (1) Berg Aukas-type Zn-Pb deposits in carbonates; (2) Tsumeb-type Pb-Cu-Zn-Ge deposits in carbonates; (3) Abenab-type vanadium deposits in geologically young karst pipes and breccias; and (4) Tschudi-type low-grade Cu ores in sandstone and conglomerates of the basal Mulden Group [3]. Among these, the Berg Aukas- and Tsumeb-types, both hosted by carbonate rocks of the Otavi Group, are the economically most important mineral deposits. Berg Aukas-type deposits are considered to have formed either before the Pan-African Orogeny (as Mississippi Valley-type MVT mineralization [4,5]) or during the Pan-African Orogeny [6]. Tsumeb-type deposits should instead derive from hydrothermal fluids generated during prograde metamorphism of the Pan-African Orogeny, which migrated along Pan-African faults, forming Pb-Cu-Ge-sulfide ores in discordant breccia pipes [4]. In the OML, later secondary alteration processes (both hypogene and supergene) transformed parts of the original sulfide bodies into nonsulfide ores [7,8]. In the Tsumeb and Berg Aukas area, nonsulfide ores consist of various oxidized Zn-Pb-Cu-minerals, like carbonates, silicates, phosphates, vanadates and many others [2]. Germanium is also locally remobilized in both the hydrothermal or supergene oxidized minerals, like willemite or Fe-oxy-hydroxides, and also forms proper secondary minerals (e.g., stottite [9,10]). In the northeast extension of the Namibian Damara Belt in northwest Botswana, to our knowledge, only few Zn-Pb > (Cu-Ag-V-Ge) mineralizations have been already identified. These are represented by the Kihabe and Nxuu prospects, both owned by Mount Burgess Mining N.L. These exploration projects are located in the Aha Hills (Ngamiland District), near the Dobe border gate with Namibia (Figures 2 and 3). The Kihabe prospect contains Zn-Pb resources (compliant to the 2004 Australasian Code for Reporting of Exploration Results, Mineral Resources and Ore Reserves – JORC code) of 14.4 million tons at 2.84% zinc equivalent, and an Ag amount of 3.3 million ounces. The Nxuu Zn-Pb resources are currently estimated at around 10.9 million tons at 3.20% zinc equivalent. Even though V and Ge have been detected in both prospects, these elements have not been included yet in the resource estimate [11]. The Kihabe and Nxuu mineralizations consist of mixed sulfide–nonsulfide bodies hosted in Neoproterozoic rocks. In this paper, we present the results of a mineralogical and geochemical study, conducted on drillcore samples of the Kihabe prospect, delineating a possible genesis of its sulfide–nonsulfide ores, in comparison with similar mineral deposits located in the region.

2. Geological Setting

2.1. Regional Geology

In the Ngamiland District, the Pan-African Damara Belt extends from Namibia in the SW, northwest Botswana to Zambia and Congo in the NE (Figure 1; [12]). As most of the Precambrian basement is covered by a blanket of Kalahari sedimentary rocks and various lithotypes belonging to the Karoo Supergroup, the reconstruction of its tectonic framework is partly unclear, and mostly based on the interpretation of geophysical data [12–18]. The study area is located northwest of the Ghanzi–Chobe zone, a NE-trending Meso- to Neoproterozoic belt, formed following the tectonic inversion of the Northwest Botswana rift, during the Damara Orogenesis (Figure 2; [12]). Within this domain, the younger rocks comprise clastic and carbonate lithotypes of the Ghanzi Group, which has been correlated with the Tsumis and Nosib groups in southwest Namibia [17,19–21].

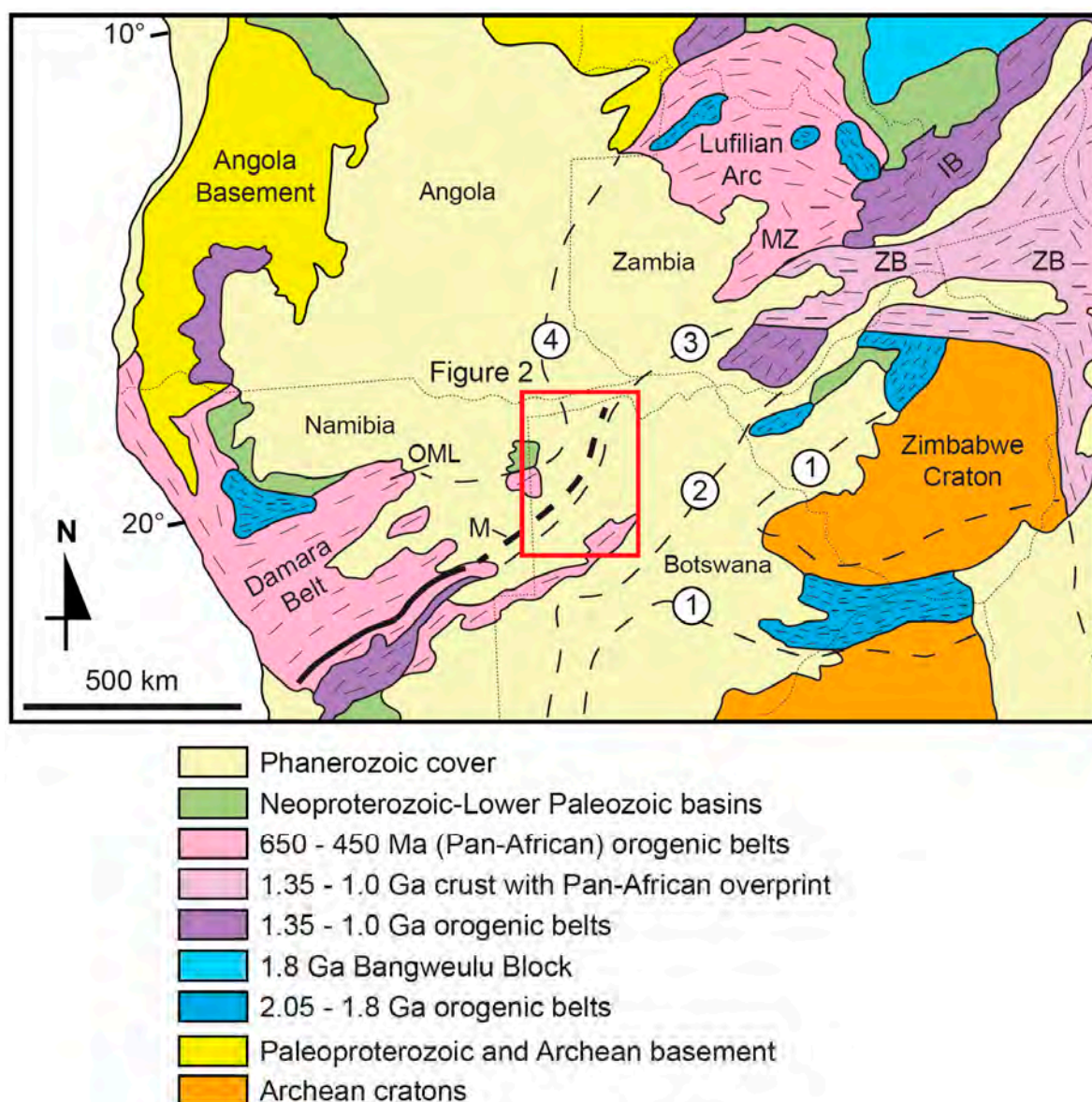


Figure 1. Precambrian tectonic framework of Southern Africa (modified from [22]). ① western edge of Archean cratons; ② boundary between 2.05–1.8 Ga orogenic belts and 1.35–1.0 Ga belts; ③ boundary between 1.35–1.0 Ga belts and Pan-African belts; ④ western edge of Pan-African belts. IB = Irumide Belt; M = Matchless Belt; OML = Otavi Mountainland; ZB = Zambezi Belt. The red square indicates the position of map in Figure 2.

Following Key and Ayers [13] and Singletary et al. [17], the basement occurring in the Ngamiland District, northwest of the Ghanzi–Chobe zone, consists of four units (Figure 2):

(1) the Kwando Complex, a geophysically distinct subsurface terrain, likely consisting of granite gneiss (of uncertain Precambrian age);

(2) a domain, which is considered to be the NE extension of the main part of the Damara Belt in Botswana [12], characterized by northeast-structural trending meta-sedimentary and meta-igneous rocks. This domain is composed of four juxtaposed terrains: (i) the Roibok Complex (amphibolite and mafic schists, correlated with the Neoproterozoic Matchless Belt of southern Damara Orogen [23]); (ii) the Koanaka Group (Neoproterozoic), consisting of strongly deformed, greenschist-facies meta-sedimentary rocks and marbles outcropping in the Kihabe and Koanaka Hills [12,13]; (iii) the Chihabadum Complex (Neoproterozoic?), made up of igneous and meta-igneous rocks; and (iv) the lower grade Aha Hills

Formation (Neoproterozoic; [13]), consisting dominantly of chert-rich marble and dolomite exposed in the Aha Hills, which could be correlated with the lithotypes of the Otavi Group in Namibia [12];

(3) the Quangwadum Complex (Paleoproterozoic), that is represented by a granitic-gneissic basement massif, outcropping on the northern slopes of the Aha Hills;

(4) the Xaudum and Tsodilo Hills groups, which comprise meta-sedimentary rocks characterized by strong north-to-northwest structural trends, occurring north of the Quangwadum Complex. The Xaudum Group is composed of folded, low metamorphic grade fine-grained marbles, carbonate rocks with chert, quartzites and slates. The Tsodilo Hills Group comprises kyanite-grade quartz–muscovite schists, meta-conglomerates, ferruginous quartzites and biotite-gneisses. The groups are considered to have either a Paleoproterozoic [13] or a Neoproterozoic age [17]. In greater detail, Singletary et al. [6] correlate the Xaudum Group with the Nosib Group, and the Tsodilo Hills Group with the glaciogenic rocks of the Chuos Formation of the Damara succession in Namibia.

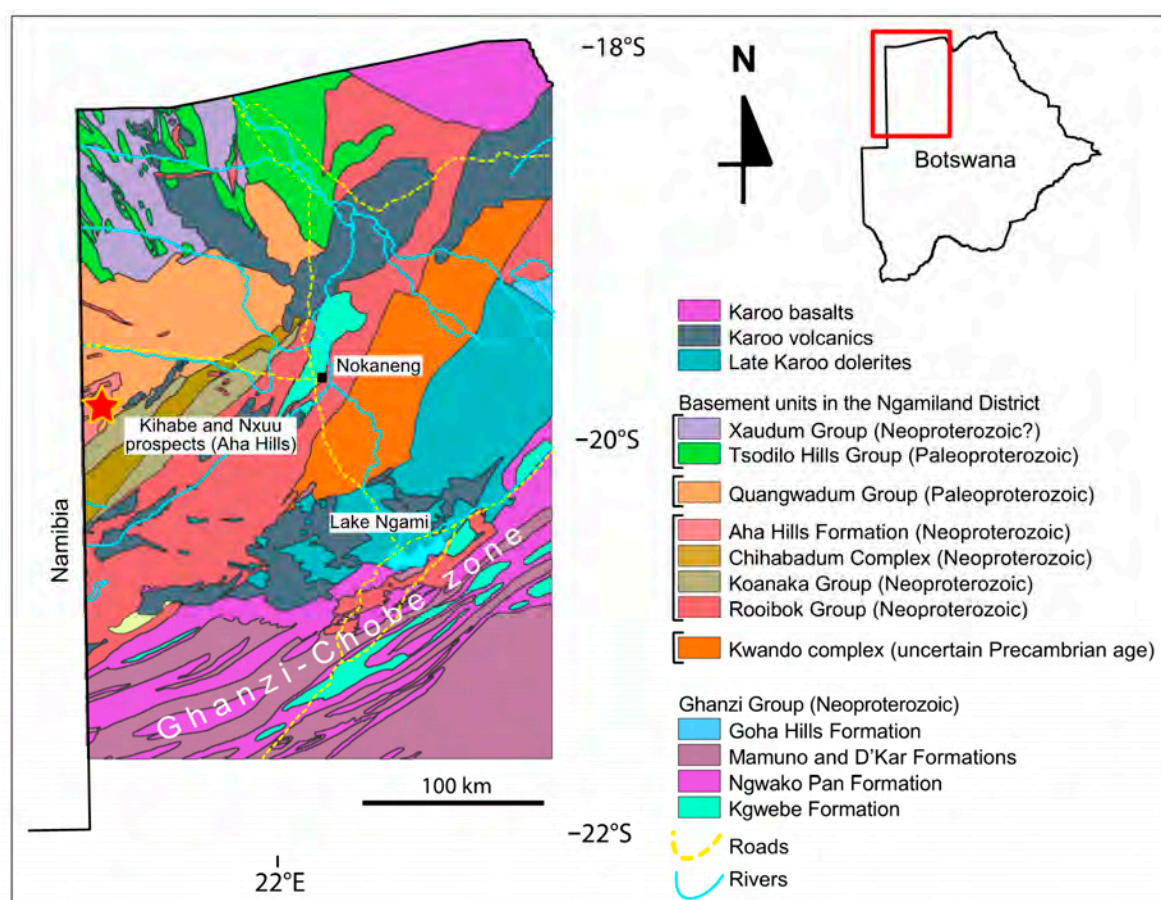


Figure 2. Subsurface geological map of northwestern Botswana, with the location of the Kihabe and Nxuu prospects (modified from [13]). The Kalahari cover is not shown.

According to other authors (e.g., [15] and references therein), the meta-sedimentary successions occurring in the Ngamiland District, both to the north and to the south of the granitic–gneissic Quangwadum Complex, have to be subdivided into only two units: the Xaudum Group and the Tsodilo Hills Group. The Xaudum Group is considered to be a part of the Ghanzi–Chobe Supergroup together with the Roibok Formation and the Ghanzi Group, and should have a Neoproterozoic age. The Tsodilo Hills Group has instead a Paleoproterozoic age (after zircon dating; [15]), and thus predates the Xaudum Group and the other meta-sedimentary rocks of the Damara sequence in northwest Botswana.

2.2. The Kihabe Prospect

Anomalous Zn-Pb values in the Aha Hills were detected at first during a regional geochemical survey, carried out by the Geological Survey of Botswana in the early 1980s [24]. These anomalous concentrations were later confirmed by Billiton explorative work (Grids 30-1 and 30-2; [25]), and delineated within flat valleys, characterized by a fairly thick drift cover. After having undertaken detailed geochemical surveys, the company drilling intersected some secondary pyromorphite and vanadinite mineralizations at depths ranging from 8 to 15 m within the Kalahari sedimentary rocks [26]. The anomalous Zn-Pb contents in the surficial sediments were revealed to be lying directly above the current known Kihabe mineralization.

The Kihabe prospect (Figure 3) has a strike length of 2.4 km, and could be mined with two open-cut pits covering a total length of 1.8 km. It is estimated that the two proposed pits will have strip ratios in the order of 4.5:1. Within the 1.8 km of strike, the average width of the deposit is 27 m, from 5 m below surface to 175 m depth. This depth corresponds to the maximum extent of the drillholes to date (2019; [11]). Many sections of the Kihabe resource are between 35 m and 60 m wide (Figure 4). The mineralization is covered by 5 to 15 m of Kalahari sedimentary rocks (Figure 4), and consists of stratabound orebodies hosted in a quartzwacke, at the contact with the barren dolostone, which have been deformed by folding and minor faulting (Figure 4). Following Key and Ayers [13], the host rock belongs to the Aha Hills Formation. The orebody is elongated along a general NE–SW direction and appears to be localized in steeply dipping isoclinal fold limbs (Figure 4; [27]). The sulfide mineralization at Kihabe, which represents 75% of all the ore, has been regarded as a sedimentary-hosted massive sulfide (SHMS) or Mississippi Valley type deposit [25,27]. Approximately 25% of the more surficial part of the orebody shows supergene alteration (Figure 4; [27]). Previous studies conducted in this zone revealed that Zn is mainly hosted in smithsonite and baileychlore. Lead is concentrated predominantly in galena remnants, as well as in minor Pb-oxidized minerals, whereas V is associated with descloizite [11]. Significant intersections of V have also been defined in zones outside the perimeter of the known Zn-Pb mineralization, leading to a possible expansion of the current resource area [11]. Metallurgical test work on the Kihabe sulfide ores has shown that good Zn and Pb recoveries are achieved through flotation. The Kihabe oxidized ore can instead be treated through solvent extraction and electrowinning methods (SX-EW) [11].

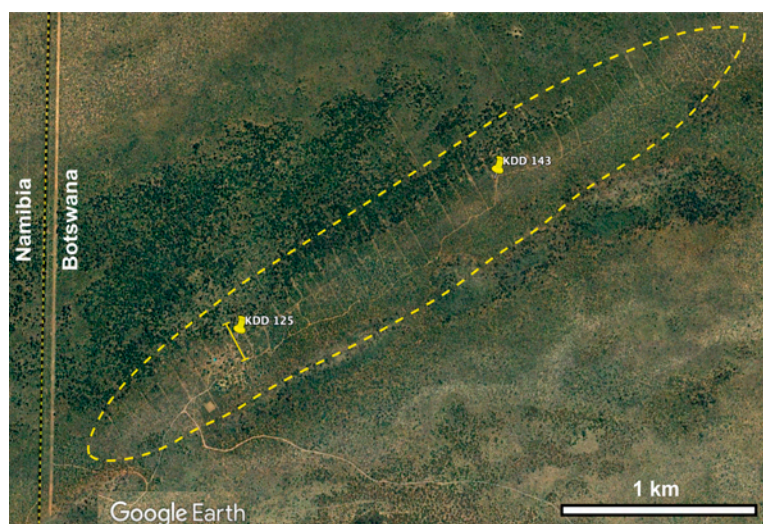


Figure 3. Satellite photograph of the Kihabe prospect (from Google Earth; image 2008), with the position of the analyzed drill holes: KDD 125: 19°42′3.81″ S latitude, 21°0′29.78″ E longitude; and KDD 143: 19°41′38.37″ S latitude, 21°1′15.71″ E longitude. The yellow dashed line represents the outline of the mineralization. In correspondence of the drill hole KDD 125, the projection of the geological section depicted in Figure 4 is indicated.

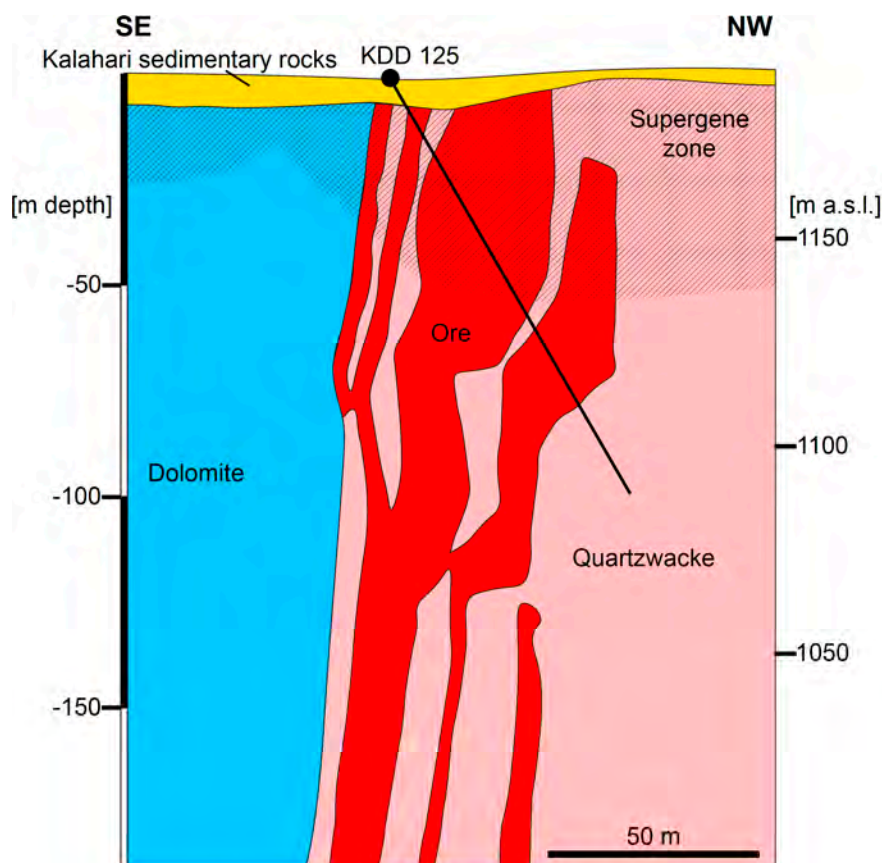


Figure 4. Schematic geological section of the Kihabe mineralized body (modified from [11]). Ore = outline of the ore bodies based on drillcore 3D modeling [11]. See Figure 3 for the location of the cross section within the prospect area.

3. Materials and Methods

For this study, we analyzed 30 samples (Table 1) collected by the Mount Burgess personnel, from two drillcores located in two distinct areas of the Kihabe project (Figures 3 and 5): KDD 125 from the southwestern zone ($19^{\circ}42'3.81''$ S latitude, $21^{\circ}0'29.78''$ E longitude; interval 55.00–60.90) and KDD 143 in the northeastern zone ($19^{\circ}41'38.37''$ S latitude, $21^{\circ}1'15.71''$ E longitude; interval 50.00–54.93).

Small slabs from the core samples have been cut, in order to get polished thin section preparations for petrographic and mineralogical analysis using conventional optical and scanning electron microscopy (SEM), equipped with energy dispersive spectroscopy (EDS). The remaining material was then crushed and homogenized for whole-rock chemical analysis and qualitative X-ray powder diffraction (XRPD).

Representative powder samples for each drillcore were obtained by first crushing the sample in a jaw crusher and then sieving to <2 mm. These fragments were then repeatedly split, using an Endecott stainless steel hand-held 50/50 sample divider (6.35 mm slot) until a ~ 20 -g representative sample was obtained. This was then milled with an agate pot and put in a Tema mill until a fine-grained powder material was obtained (30–90 s depending upon rock hardness). This powder was used for whole rock chemical analyses of major and minor elements. Whole rock chemical analyses were carried out at the Bureau Veritas Analytical Laboratories Ltd. (Vancouver, BC, Canada). The pulverized samples were subjected to LiBO_2 - LiB_4O_7 fusion (to measure SiO_2), and 4-acid digestion. The analyses were carried out by ICP-ES (multi-element inductively coupled plasma emission spectrometry)-ICP-MS (multi-element inductively coupled plasma mass spectrometry) for 41 elements. Concentrations above detection limits were obtained for 35 elements.

Table 1. List of studied drillcore samples, with mineralogy inferred by qualitative XRPD.

Drillcore	Sampled Interval	Sample Label	Mineral Assemblage
KDD125	55.00–55.34	KDD 125-1	Qz, Ms, Cer
	55.34–55.76	KDD 125-2	Qz, Ms, Ang
	55.76–56.05	KDD 125-3	Qz, Ms, Ang, Sp, Hem
	56.05–56.50	KDD 125-4	Qz, Ms, Sp, Gn, Py
	56.60–57.00	KDD 125-5	Qz, Ms, Sp, Gn, Py, Hem
	57.00–57.30	KDD 125-6	Qz, Ms, Sp, Gn, Sm, Py, Hem
	57.30–58.07	KDD 125-7	Qz, Ms, Or, Cer, Gn, Sm
	57.08–58.57	KDD 125-8	Qz, Ms, Sm, Sp, Gn, Hem
	58.57–58.89	KDD 125-9	Qz, Ms, Sp, Gn, Hem
	58.89–59.10	KDD 125-10	Qz, Ms, Sp, Gn, Py
	59.10–59.96	KDD 125-11	Qz, Ms, Sp, Gn, Py, Hem
	59.96–60.10	KDD 125-12	Qz, Ms, Hem
	60.10–60.32	KDD 125-13	Qz, Ms, Sp, Gn, Sm, Hem
	60.32–60.63	KDD 125-14	Qz, Ms, Or, Kln, Gn, Cer
	60.63–60.90	KDD 125-15	Qz, Ms, Or, Gn, Cer
KDD143	50.00–50.04	KDD 143-16	Qz, Ms, Sm, Wlm
	50.04–50.40	KDD 143-17	Qz, Ms, Sm, Wlm, Hem
	50.40–50.72	KDD 143-18	Qz, Ms, Or, Sm, Blc, Cer
	50.72–50.92	KDD 143-19	Qz, Ms, Or, Sm, Blc
	50.92–51.24	KDD 143-20	Qz, Ms, Or, Sm, Blc, Hem
	51.24–51.60	KDD 143-21	Qz, Sm, Ms, Blc, Ill, Or
	51.60–51.86	KDD 143-22	Qz, Ms, Or, Sm, Blc, Ill
	51.86–52.20	KDD 143-23	Qz, Sm, Ms, Or, Blc, Wlm, Mim, Cer
	52.20–52.55	KDD 143-24	Qz, Sm, Ms, Blc, Mim, Cer, Or
	52.55–52.72	KDD 143-25	Qz, Blc, Or, Ms, Cer, Sau, Ill
	52.72–53.00	KDD 143-26	Qz, Blc, Or, Ms, Cer, Sau, Ill, Wil, Sm
	53.00–53.93	KDD 143-27	Qz, Ms, Or, Blc, Cer
	53.93–54.26	KDD 143-28	Qz, Ms, Blc, Sm
	54.26–54.65	KDD 143-29	Qz, Ms, Cer, Gn, Sm
	54.65–54.93	KDD 143-30	Qz, Ms, Cer, Gn, Sm, Wlm

Minerals are listed in order of abundance, qualitatively evaluated on the basis of bulk rock chemical compositions. Ang = Anglesite; Blc = baileychlorite; Cer = cerussite; Gn = galena; Hem = hematite; Ill = illite/smectite (inferred with the support of SEM-EDS; see text for details); Kln = kaolinite; Mim = mimetite; Ms = muscovite; Or = orthoclase; Py = pyrite; Qz = quartz; Sau = sauconite; Sm = smithsonite; Sp = sphalerite; Wlm = willemite.



Figure 5. Pictures of drillcore trays with the analyzed drillcore intervals (enclosed in the red line): KDD 125: interval 55.00–60.90; and KDD 143: interval 50.00–54.93. In both the cores it is possible to see reddish intervals, affected by supergene alteration.

X-ray powder diffraction (XRPD) analysis for mineral phase identification was carried out on identical powder splits to those used for whole rock chemical analyses. X-ray powder diffraction analysis was carried out at the Institute of Earth Sciences, Heidelberg University (Germany), with a Siemens D 500 Bragg-Brentano X-ray diffractometer, with $\text{CuK}\alpha$ radiation, 40 kV and 30 mA, 5 s/step and a step scan of $0.05^\circ 2\theta$. The data were collected from 3 to $110^\circ 2\theta$. Relative abundances between the minerals were qualitatively determined on the basis of the bulk rock chemical analyses of the samples, and the chemical compositions of identified minerals.

The thin sections were firstly examined under a petrographic microscope with both transmitted and reflected light. Scanning electron microscopy observations and back-scattered electrons (BSE) imaging were carried out on selected polished thin sections from material with the highest metallic grades. The carbon-coated sections were analyzed with a JEOL JSM5310 instrument at the University of Napoli. Element mapping and qualitative EDS spectra were obtained by the INCA microanalysis system equipped with an Oxford energy dispersive spectrometry INCA X-stream pulse processor and the 4.08 version Inca software. The operating conditions were an acceleration voltage of 15 kV, 50–100- μA filament current, variable spot size and a working distance of 20 mm. The reference standards used for quantitative microanalysis were anorthoclase, Si, Al and Na; diopside, Ca; microcline, K; rutile, Ti; fayalite, Fe; olivine, Mg; serandite, Mn; sphalerite, Zn; benitoite, Ba; celestite, Sr; fluorite, F; halite, Cl; pyrite, S; galena, Pb; and pure metal, Cu. Detection limits of the analyzed elements are below 0.1%.

4. Results

Sulfides were detected preferentially in the drillcore KDD 125, whereas oxidized minerals occur in both analyzed cores. Willemite and baileychlore were detected only in core KDD 143 (Figure 6; Table 1; Table 2). The meta-quartzwacke host rock is characterized by abundant fine-grained quartz and minor feldspar clasts (Table 1), with an intergranular matrix made up of micas and other phyllosilicates, some occurring as distinctly schistose muscovite aggregates, and some others showing a finer decussate structure (Figure 7a–d). Micas have a muscovite composition, with minor amounts of Mg (ca. 1 wt. % MgO). Fine newly-formed silica (silicification) has also been observed. The quartzwacke contains several types of detrital minerals in traces, like ilmenite, rutile, monazite, tourmaline and zircon.

Table 2. Summary of the ore minerals detected in the Kihabe samples, with their International Mineralogical Association (IMA)-accepted chemical formulas.

Mineral	Formula
Anglesite	PbSO_4
Argentite	Ag_2S
Baileychlore	$(\text{Zn,Fe}^{2+},\text{Al,Mg})_6(\text{Si,Al})_4\text{O}_{10}(\text{OH})_8$
Cerussite	PbCO_3
Galena	PbS
Hemimorphite	$\text{Zn}_4(\text{Si}_2\text{O}_7)(\text{OH})_2\cdot\text{H}_2\text{O}$
Hinsdalite	$\text{PbAl}_3(\text{SO}_4)(\text{PO}_4)(\text{OH})_6$
Iodargyrite	AgI
Mimetite	$\text{Pb}_5(\text{AsO}_4)_3\text{Cl}$
Pyromorphite	$\text{Pb}_5(\text{PO}_4)_3\text{Cl}$
Sauconite	$\text{Na}_{0.3}\text{Zn}_3(\text{Si,Al})_4\text{O}_{10}(\text{OH})_2\cdot 4\text{H}_2\text{O}$
Smithsonite	ZnCO_3
Sphalerite	ZnS
Willemite	Zn_2SiO_4

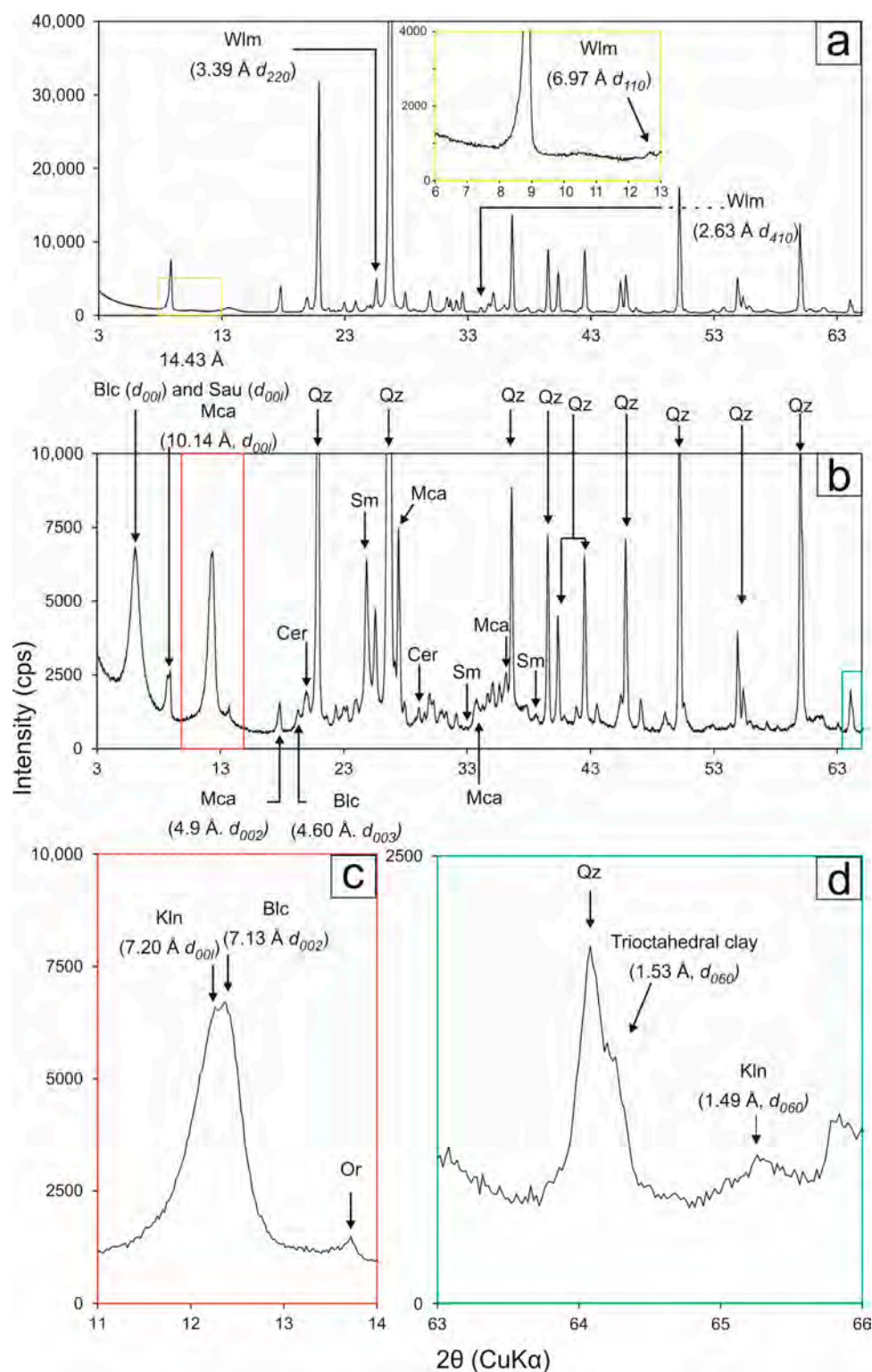


Figure 6. Examples of XRPD patterns of willemite- and baileychlore-bearing samples: (a) Sample KDD143-16: XRPD pattern showing characteristic peaks of willemite (other minerals identifiable in the pattern are quartz, muscovite and smithsonite; see Table 1); (b) Sample KDD143-26: XRPD pattern showing characteristic peaks of major phases occurring in the sample; (c) and (d) enlargements of (b) showing characteristic peaks of baileychlore. Notes: unspiked peaks in the XRPD pattern of sample KDD143-26 correspond to minor reflections of orthoclase. Blc = baileychlore; Cer = cerussite; Kln = kaolinite; Mca = mica (undistinguished; see text for details); Or = orthoclase; Qz = quartz; Sau = sauconite; Wlm = willemite.

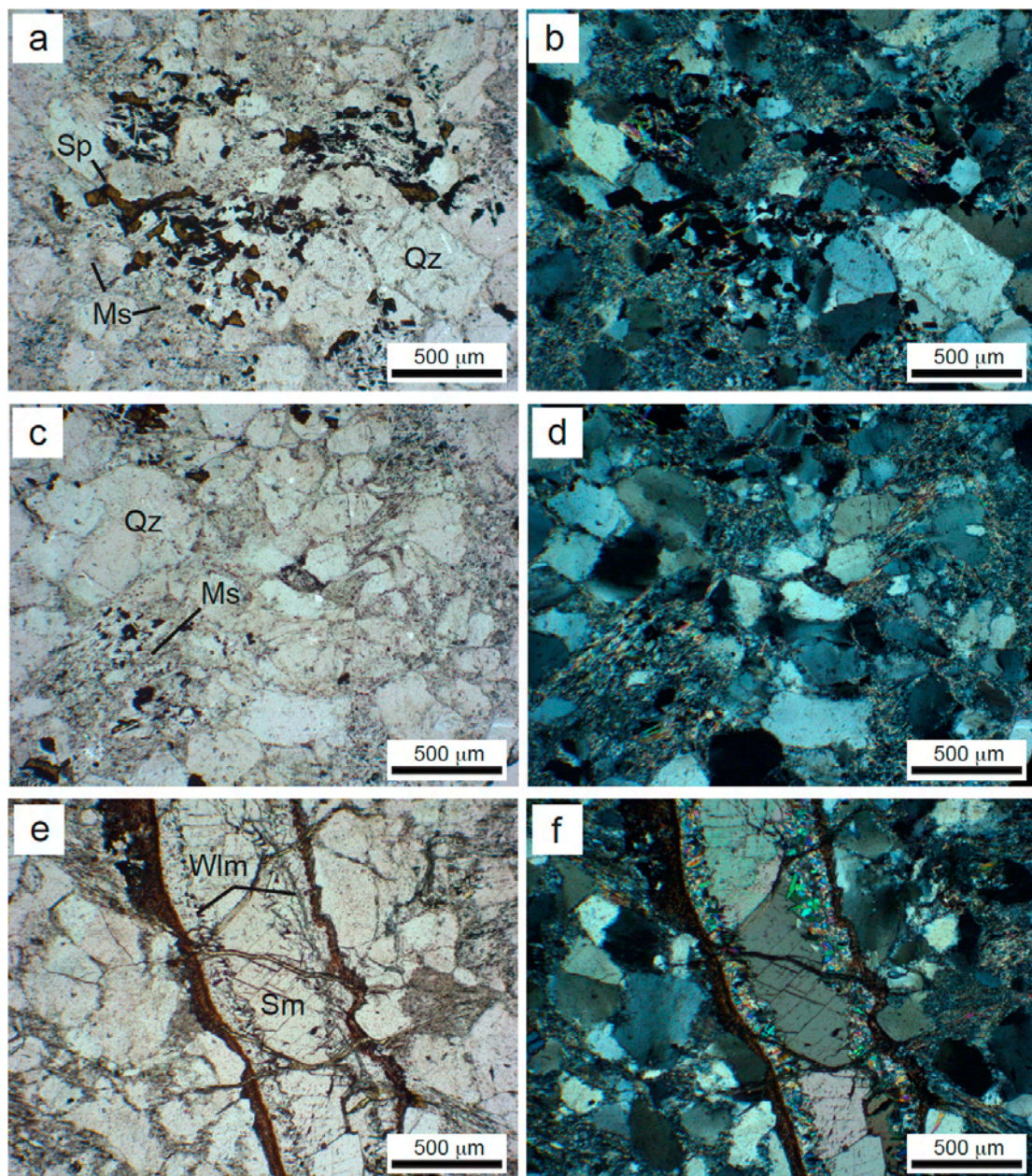


Figure 7. Transmitted light micrographs: (a) and (b) Sample KDD 125-8: Sphalerite dispersed in the quartzwacke matrix, in between micas with decussate structure (NII and N+); (c) and (d) Sample KDD 125-8: Quartzwacke with schistose structure (NII and N+); (e) and (f) Sample KDD 143-16: Vein consisting of willemite and smithsonite (NII and N+). Ms = muscovite; Qz = quartz; Sm = smithsonite; Sp = sphalerite; Wlm = willemite.

In the drillcore KDD 125, sphalerite appears to be interstitial in the quartzwacke (Figure 7a,b), intergrown with quartz and mica (Figure 8a). Locally, sphalerite is slightly ferroan (3–4 wt. % Fe) and can contain up to 1–2 wt. % Pb, with subordinate As (0.3 wt. %). Galena occurs either at the rim of the sphalerite crystals or in the porosity of the host rock (Figure 8a,b). Pyrite is relatively rare (Figure 8c), and contains variable amounts of As and Cu (rarely Co). Locally, arsenopyrite has been observed in association with sphalerite (Figure 8d). Argentite micrograins are dispersed within the above-mentioned mineral assemblage, both in the sulfides and the quartz gangue. At the microscale, sulfides appear clearly deformed, following the foliation pattern of the quartzwacke host

rock (Figure 8b). In the drillcore KDD 143, sulfides are rather rare, and only occur as local relicts within quartz cements. Barite occurs as a rare accessory phase.

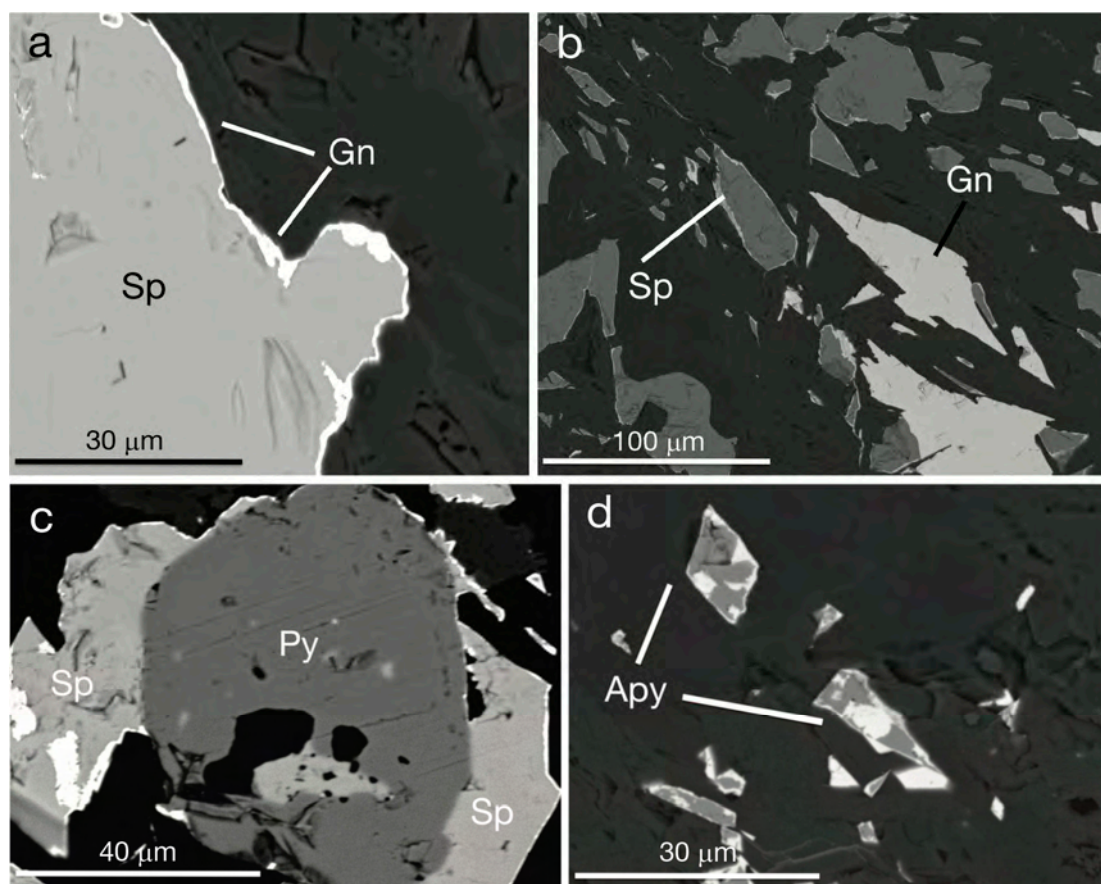


Figure 8. Backscatter electron SEM micrographs of sample KDD 125-8. Mineral chemistry was determined through EDS. (a) Sphalerite with galena border associated with quartz grains; (b) Sphalerite and galena elongated within the quartzwacke; (c) Pyrite grain associated with sphalerite; (d) Arsenopyrite intergrown with As-rich sphalerite. Apy = arsenopyrite; Gn = galena; Py = pyrite; Sp = sphalerite.

Willemite has been detected via the XRPD and by observation of thin sections (Table 1; Figures 6a and 7e,f). It occurs as patches and/or vein filling (Figure 7e,f and Figure 9a–d), forming two generations: the first one generally forms small allotriomorphic masses, as a cement of the host rock (Figure 9a) and appears slightly deformed, whereas the second generation forms euhedral micro- to macro-crystals in veins and cavities, and does not show peculiar deformation structures (Figure 9b,c). Both willemite generations can be As-rich (up to 2.5 wt. % As_2O_5 ; Table A1).

Among the sampled cores, baileychlore is only present in the willemite-bearing samples (Table 1). The Zn-chlorite was identified with the XRPD method, through the characteristic d_{hkl} peaks at 14.290 Å (d_{001}), 7.145 Å (d_{002}) and 1.53 Å (d_{060}) (Figure 6b–d; [28]). This Zn-bearing chlorite texturally grows in the porosity of the country rock, upon and between preexisting mica packages, and it appears to locally replace K-feldspar (Figure 10a–e). In some cases, when baileychlore substitutes K-feldspar, it is texturally associated with kaolinite and galena (Figure 10b,c).

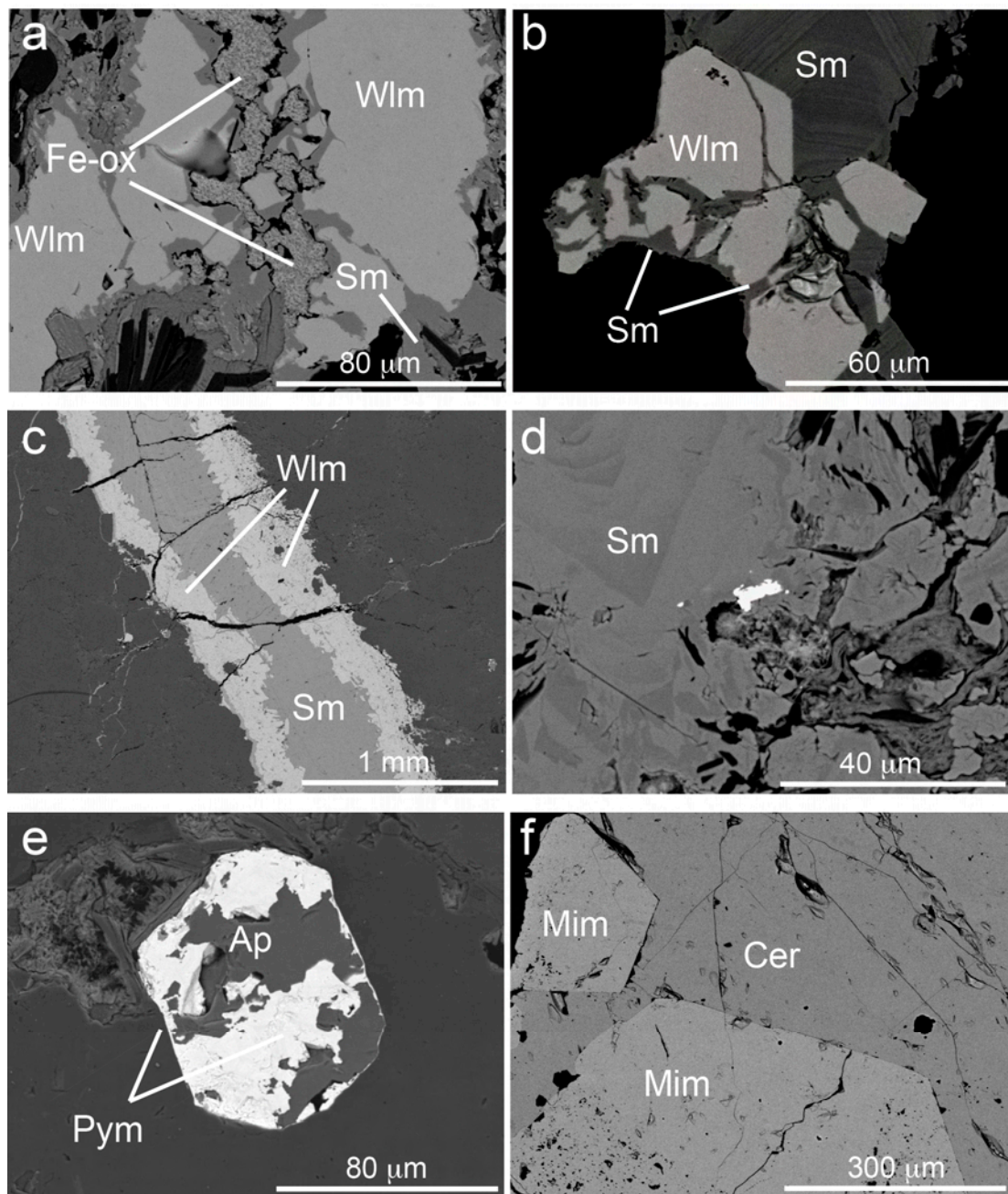


Figure 9. Backscatter electron SEM micrographs. Mineral chemistry was determined through EDS. (a) KDD 143-22. Willemite altered and partially replaced by smithsonite and Fe-oxy-hydroxides; (b) KDD 143-23. Idiomorphic willemite crystals, vein-crossed and partially altered to zoned smithsonite; (c) KDD 143-16. Thin willemite vein, internally filled with smithsonite; (d) KDD 143-16. Zoned crystals of smithsonite; in the center small galena remnant; (e) KDD 143-26. Fluorapatite crystal patchily replaced (Pb → Ca and Cl → F) by pyromorphite; (f) KDD 143-23. Idiomorphic mimetite crystals embedded in cerussite. Ap = fluorapatite; Cer = cerussite; Fe-ox = Fe-oxy-hydroxides; Mim = mimetite; Sm = smithsonite; Wlm = willemite.

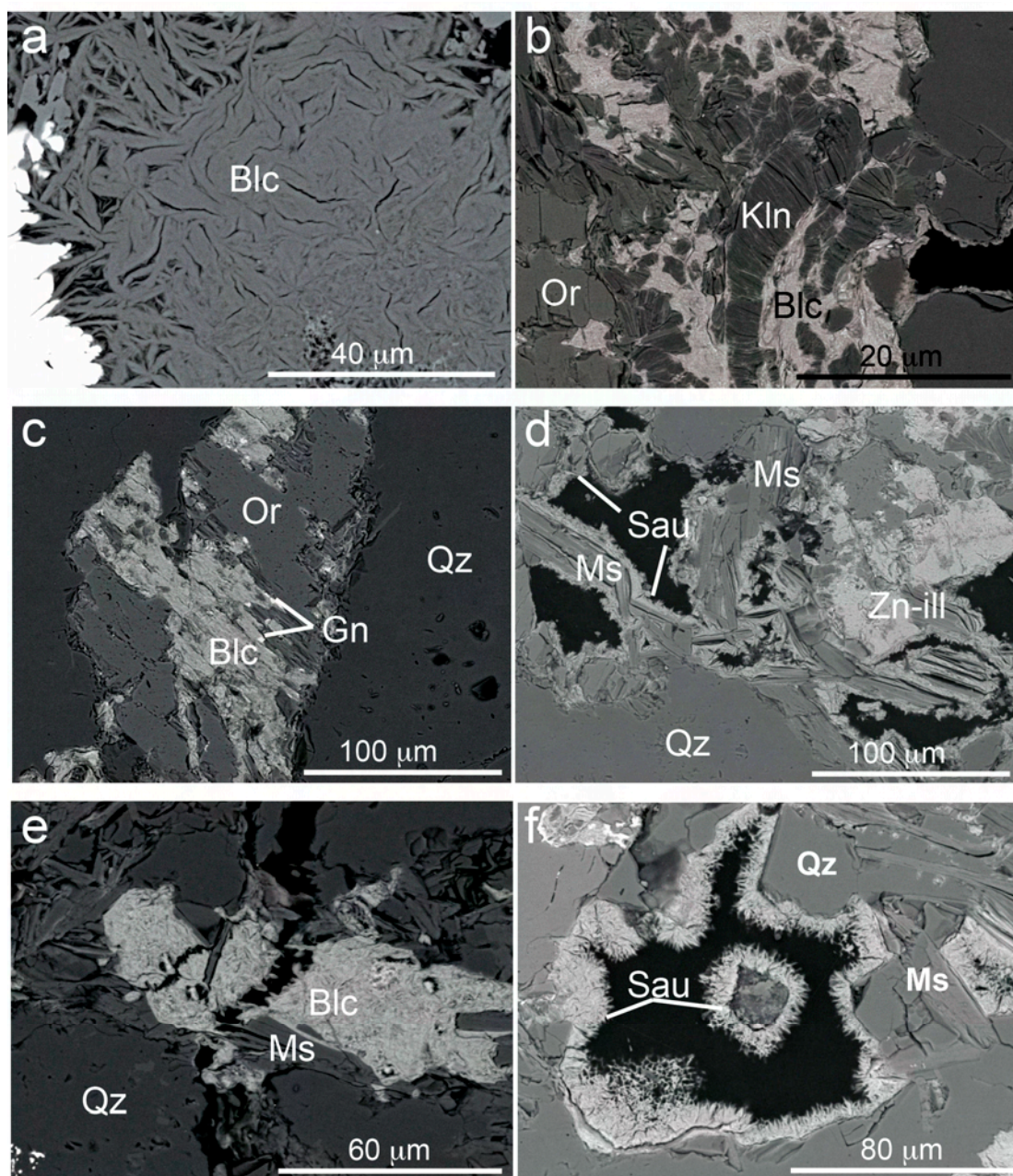


Figure 10. Backscatter electron SEM micrographs. Mineral chemistry was determined through EDS. (a) KDD 143-23. Baileychlore packages, randomly oriented, filling porosity; (b) KDD 143-22. Baileychlore associated with kaolinite replacing orthoclase; (c) KDD 143-26. Orthoclase crystal from the host quartzwacke partially replaced by baileychlore; fine galena is associated with the Zn-chlorite; (d) KDD 143-26. Sauconite and Zn-bearing illite growing in dissolution cavities, above mica packages; (e) KDD 143-22. Patches of baileychlore growing in between mica packages and quartz grains; (f) KDD 143-26. Dissolution cavity bordered by freely growing sauconite. Blc = baileychlore; Gn = galena; Kln = kaolinite; Ms = muscovite; Or = orthoclase; Qz = quartz; Sau = sauconite; Sm = smithsonite; Zn-ill = Zn-bearing illite.

Differently from the compositional data quoted in the literature (Table A2; [28]), the zinc content of the Kihabe baileychlore is higher, ranging from 37.5 to 47.6 wt. % ZnO, and is associated with MgO values varying between 1.5 and 3.5 wt. %, slightly lower Al₂O₃ contents between 10 and 16 wt. %, and SiO₂ between 26 and 31 wt. %. The Kihabe baileychlore has relatively low FeOt contents (< 1 wt. %) (Table A2). In a few analyses, Cu concentrations of ca. 1 wt. % have been detected. Although

SEM-EDS is not the best method for measuring the chemical composition of phyllosilicates, based on the mentioned chemical composition, baileychlore structure formulae calculated for 28 oxygen equivalents do not give results very different from the IMA-accepted formula (Table A2; [28]). Si has an average value of 3.47 apfu, and Al^{VI} is on average 1.30 apfu, whereas Mg ranges between 0.28 to 0.63 apfu, and Zn between 3.20 and 4.28 apfu. Iron, evaluated as Fe²⁺, has a maximum occupancy of 0.17 apfu. Among these data, the calculated Si apfu show no variation respect to Zn apfu, whereas there are clear inverse correlations between Si and R²⁺ (Zn, Fe, Mg) apfu and Al^{VI} apfu (Table A2). Among the other phyllosilicates, sauconite occurs as a late-stage phase growing in cavities, and is commonly associated with Zn-bearing illite. The last one probably consists of illite/smectite (sauconite) mixed layers (e.g., sample KDD 143–26; Figures 6b and 10e,f).

Smithsonite occurs in two generations in both the analyzed cores. In the first generation, it appears as a local replacement of sphalerite or willemite, and shows minor As amounts retained from the altered Zn-silicate (Figure 9a,b). A second smithsonite phase forms concretions in cavities and fills pore spaces in the host rock (Figure 9c,d). This concretionary smithsonite is commonly chemically zoned (Figure 9d), with alternating bands containing variable Mg amounts (up to 4 wt. % MgO, Table A1).

Cerussite is the most common oxidized Pb-mineral at Kihabe in both the analyzed cores (Table 1), though it occurs in small patches and locally, as euhedral crystals in association with Fe-oxy-hydroxides. It may contain small amounts of Zn. Anglesite was detected in traces only by XRD (Table 1). Pyromorphite occurs as cement in the country rock or as replacements along the rims of fluorapatite (Figure 9e; Table A3). Mimetite locally occurs as euhedral crystals intergrown with cerussite (Figure 9f), and contains small amounts of phosphorus (Table A3). Hinsdalite was also detected in a couple of samples (KDD 125-5 and KDD 143-26). Silver is present as argentite inclusions in silica, but also in iodargyrite (Ag-iodide). Iron- and Mn-oxy-hydroxides, containing small amounts of Zn, Pb and Si, are widespread in both the cores (Tables 1 and A3).

Even though descloizite is reported by Mt Burgess Ltd. [11], as an abundant mineral in the most surficial section of the ore, this vanadate was not detected neither through XRPD nor at SEM-EDS in the samples analyzed for this study.

The results of the chemical analyses of 20 selected Kihabe samples are displayed in Table A4. Zinc shows values varying from <0.1% to 9% throughout the analyzed samples, with the highest concentrations in the KDD 143 drillcore. Lead is less enriched, with values ranging between 0.20% and 4.80%. Silver (8–113 mg/kg) is not strictly correlated with Pb, but is quite scattered in the samples with relatively high Pb values. Cadmium correlates with zinc, both in primary sulfides and in nonsulfides. Copper does not show high concentrations (4 to 1831 mg/kg), but its values are more abundant in the KDD 143 samples. Cobalt is relatively low, with the higher values (up to 32 mg/kg) found again in KDD 143. The As values range between 40 and 3.6 mg/kg. Vanadium reaches 260 mg/kg only in one of the examined samples, possibly indicating the presence of descloizite.

5. Discussion

The results of this study on the Kihabe prospect shed new light on the mineralizing processes, which occurred in northwestern Botswana, and on their correlation with ore deposit formation in the Namibian Damara Belt. Firstly, the Kihabe prospect hosts significant sulfide mineralization, mainly consisting of Fe-sphalerite and galena, finely disseminated in stratabound horizons within the meta-quartzwacke. The mineralization shows distinct deformation features both at the macroscale [27] and microscale, thus suggesting that sulfide emplacement occurred before or contemporaneously with the Damara Orogeny in the whole region (540–520 Ma, Figure 11; [29]). Considering that the sulfides host rock (the Aha Hills Formation) has been correlated with the Otavi Group in Namibia [17], it is possible to compare the Kihabe prospect with the ore deposits of the OML. Specifically, the orebodies in the Kihabe prospect have features in common with the Berg Aukas-type base metal deposits [4,5]. These common features are as follows: the predominance of Zn on Cu, the stratabound style structure, the limited control of faults on the sulfide mineralization, and the presence of a distinct Pan-African

deformation on the sulfide assemblage [4,5]. At the same time, the most remarkable difference of the Namibian ores is found in the distinct nature of the host rock, which at Kihabe is represented by meta-quartzwacke, whereas in the Namibian ores it is dolostone. The dolostone intersected by several drillcores in the Kihabe area is barren.

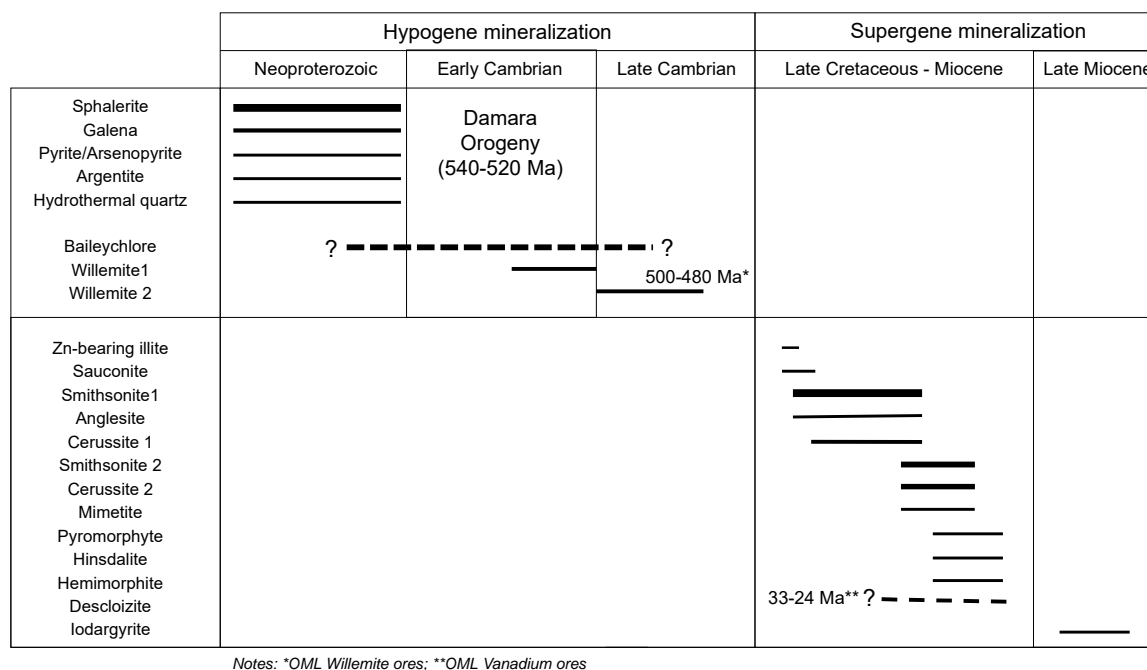


Figure 11. Mineral paragenesis of the Zn-Pb mineralization in the Kihabe area. Absolute ages after * [30], and ** [31].

In the nonsulfides assemblage, it appears that two types of mineralization styles occur in the investigated prospect: one characterized by minerals more typically found in hydrothermal ores (i.e., willemite and baileychlore; [7]), and a second one consisting of phases genetically related to real supergene processes (i.e., smithsonite, cerussite, Zn-Pb-phosphates, etc.; [7]). In detail, the presence of willemite at Kihabe is quite surprisingly, considering that the oxidized facies of the Kihabe mineralization was considered to be related to supergene alteration processes only. Specifically, two willemite types were identified: a first, deformed massive willemite generation, and a second generation consisting of euhedral hexagonal prismatic crystals. Compared to other willemite deposits [7,30,32], the Kihabe willemite should postdate sulfides emplacement, or even form at their expenses. However, we found no clear evidence of the latter process in the analyzed Kihabe samples, as is the case with the OML deposits [30]. Accordingly, this Zn-silicate could have originated either from the interaction of late-oxidizing hydrothermal fluids with preexisting sulfide bodies, or from the direct precipitation from Zn-bearing oxidizing fluids, focused along tectonic lineaments in formerly mineralized areas. The Kihabe willemite assemblage has many similarities with the willemite occurrences described in the Berg Aukas deposit [30]. In fact, the various willemite generations recorded at Berg Aukas have been comprehensively classified as (i) early willemites, occurring as fine-crystalline to granular masses replacing sphalerite, and (ii) later willemites, taking the form of semi-massive microcrystalline masses of hexagonal crystals. Absolute dating of the second willemite generation at Berg Aukas, carried out with the Rb-Sr geochronological method [30], produced ages which yield 499 ± 63 Ma and 493 ± 2 Ma, suggesting that its formation in the Otavi Mountainland was related to hydrothermal circulation during the waning stages of the Damara Orogeny, similarly to other structurally-controlled willemite mineralizations in Southern Africa (e.g., the Kabwe deposit [33,34]). Looking at the various mineralizing events that occurred in the Otavi Mountainland, it is likely that the Kihabe willemites formed in the same period (Figure 11), during the final stages of the Damara Orogeny [30]. However,

the high As concentration in the Kihabe willemite seems to be a peculiarity of this mineralized prospect, since this element rarely reaches maximum amounts of 1 wt. % in willemite, in particular structurally-controlled deposits, like Star Zinc, in Zambia [10]. The presence of As in the Kihabe willemite could be a result of the alteration of As-bearing sulfides (i.e., arsenopyrite), or could even indicate that the investigated Zn-silicate had a relatively high precipitation temperature (between 150 and 250 °C; [10]).

Baileychlore is common in the Kihabe KDD 143 core, particularly in those intervals containing willemite, whereas it is absent in the sulfide-bearing samples of the KDD 125 core. This Zn-bearing chlorite was identified for the first time by Rule and Radke [28] in the Red Dome deposit (North Queensland, Australia), a base- and precious-metal mineralization associated with calcsilicate skarn. In the above deposit [28], baileychlore occurs as a replacement of andesite and garnet-vesuvianite skarn clasts, occurring in a marble breccia. Although baileychlore was compared with other “similar” 14 Å-Zn-phyllsilicates identified in the high-T metamorphic Franklin deposit (New Jersey, UJ, USA), a supergene origin was postulated for the Red Dome Zn-chlorite [28]. Another more relevant baileychlore occurrence has been recently identified in the Prairie Downs volcanic-hosted massive sulfide (VHMS)-to SHMS-type Zn-Pb-(Cu-Ag) deposit, located in northwest western Australia [35]. In this deposit, baileychlore can be found in a broad alteration halo, extending also for more than 100 m in metabasalts surrounding the massive sulfide bodies [35]. Apparently, in the Prairie Downs deposit, baileychlore is not localized within the sulfide ore zone, but only at the border between the mineralization and the host rock, as well as in the barren zone around the orebody [35]. As in the case of VHMS deposits [36,37], this distribution was interpreted to be derived from the progressive migration of hydrothermal fluids through the porosity of the host rocks, laterally from the main feeder of the mineralization [35]. Specifically, in the Prairie Downs deposit, the Zn-chlorite was considered to have formed together with muscovite, as an alteration product of a clinozoisite–quartz protolith, developed from ZnCl₂- and KCl-rich hydrothermal fluids genetically related to sulfide mineralization [35]. The Kihabe mineralization seems to share a few similarities with the Prairie Downs deposit, in particular: (1) the spatial distribution of the baileychlore outside the sulfide ore zone, and (2) its scattered distribution throughout the host rock. It is more difficult, however, to find other analogies with Prairie Downs at the level of the deposit-type or the regional processes.

Going in detail into the microscopic structure of Kihabe baileychlore, this Zn-bearing chlorite appears to have mostly grown within the porosity, on top and in between preexisting mica packages. Baileychlore seems to replace the preexisting K-feldspars in the analyzed samples only to a limited extent. In some cases, where baileychlore substitutes for K-feldspar, it can be associated with kaolinite and galena. The porosity-filling and overgrowth textures can be considered as related to the direct precipitation of chlorite from solutions, where the preexisting 10 Å-phyllsilicates only acted as templates for the epitaxial or random crystallization of 14 Å-phyllsilicate on cleavage surfaces [38,39]. On the contrary, the substitution of feldspars might indicate a dissolution–crystallization mechanism, which could have been mediated by kaolinite. The latter mineral could represent either an intermediate phase of the replacement process, or a co-product derived from feldspar alteration. As it appears that the chlorite occurring in low-temperature systems derives from specific clay precursors through solid-state transformation mechanisms [38], whereas both direct precipitation and dissolution–crystallization processes are typical of hydrothermal systems [40], the textures described in the analyzed samples strongly suggest that Kihabe baileychlore is associated with the same hydrothermal processes that were responsible for the mineralization. To our knowledge, a specific geothermometer for baileychlore does not exist. However, by using the graphical semiempirical chlorite geothermometer of Bourdelle and Cathelineau [41], based on the Si and R²⁺ occupancy (in this case, we used the analyses obtained with SED-EDS; see values in Table A2), we estimated temperatures between 50 and 150 °C (Figure 12).

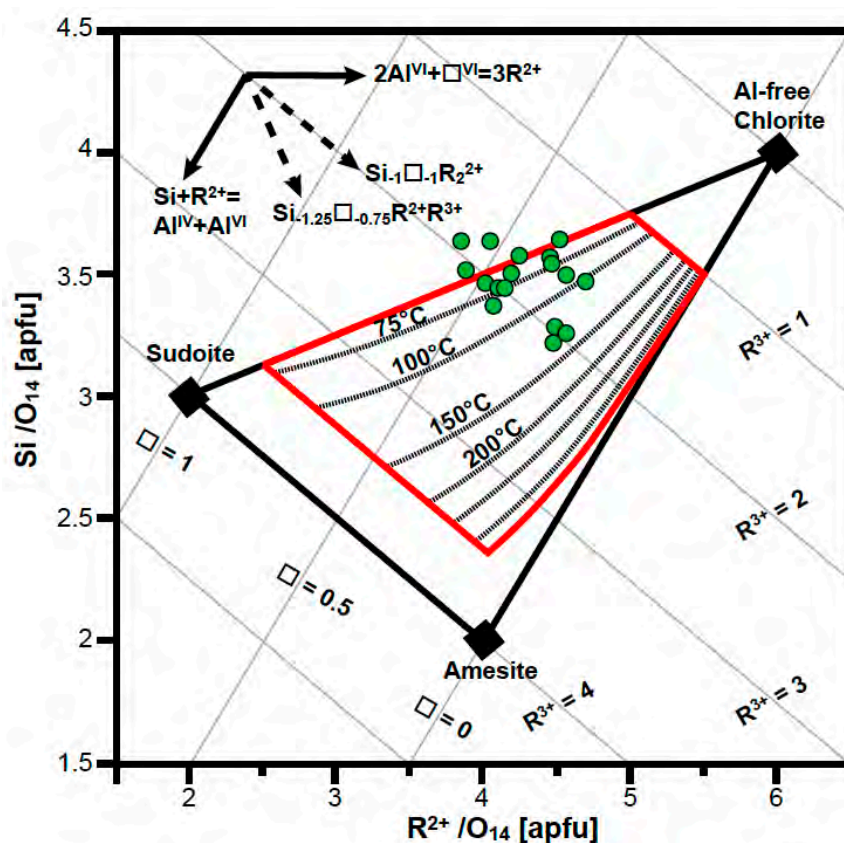


Figure 12. Semi-empirical graphical chlorite geothermometer of Bourdelle and Cathelineau [41], applied on the baileychlorite analyses obtained with this study. In the top-left corner, the element substitution vectors are shown.

Although the above data must be considered with the utmost care, because the geothermometer is not calibrated on baileychlorite and the analyses were carried out with the EDS method, at a rough scale the values are in agreement with the theoretical hydrothermal genesis of the Kihabe Zn-chlorite. This would also be coherent with the paragenetic association of baileychlorite with willemite. This considered, the peculiar association of baileychlorite with galena (and kaolinite), observed where the Zn-chlorite replaces feldspar, could be related to the cooling and neutralization of the acidic species ZnCl^+ and PbCl^+ during the infiltration of the hydrothermal fluid into the country rock, following a process well-described for the propylitic alteration bands around porphyry Cu systems [42], which produces assemblages of chlorite and sulfides in traces similar to those detected at Kihabe. This textural characteristic, in conjunction with the broad similarity between the occurrence of Zn-chlorite at Kihabe and the hydrothermal halo of the Prairie Downs deposit [35], raises further questions on the origin of the Kihabe baileychlorite. Specifically, it remains still unclear if the Kihabe Zn-chlorite represents a hydrothermal alteration associated with the primary sulfide mineralization, or if it is instead genetically related to the willemite precipitation (Figure 11). In any case, it seems unlikely that baileychlorite has a supergene origin, and that it is only localized in the more surficial supergene alteration zone [11], although further analyses are required to shed more light on the last point.

In the analyzed samples, sauconite was detected only in a few samples with XRD and SEM-EDS (Table 1). Here, it occurs as a late-stage phase growing in cavities, as a replacement of baileychlorite, or included in illite–smectite mixed layers. Similar textures have been observed in the Skorpion (Namibia; [43]) and Yanque (Peru; [44]) deposits. In both cases, sauconite in cavities and overlying muscovite/illite was considered to derive from neomineralization processes. In the Skorpion deposit, the formation of sauconite at the expense of a Zn-chlorite was instead considered as related to retrograde alteration from chlorite to smectite [43]. The textural relationship differs from that observed

for muscovite, which represents a simple template on which smectite crystallizes directly from fluids. This difference of behavior between the 10 Å- and 14 Å-phyllsilicate was considered related to the fact that chlorite is more favorably subjected to chemical alteration and weathering than white mica [43]. Even though saucnite can form under a wide range of temperatures (25–200 °C) [44], considering the present data, it is probable that the Kihabe saucnite has a supergene origin.

Among the more typical supergene phases, smithsonite is common at Kihabe in both the analyzed cores, as newly-formed crystals in cavities, but also as a direct replacement of willemite. This characteristic has been observed in many willemite-bearing nonsulfide deposits [34,45–48], and was considered as related to percolation through the soil of carbonate-rich meteoric waters, which altered the preexisting Zn-silicate. In these cases, groundwaters could have become enriched in carbonate either by leaching the host rock, or by taking organic carbon from a vegetated soil [49]. Among the Pb-minerals, cerussite was formed via a similar process, whereas the Pb-phosphates (pyromorphite and hinsdalite) formed as replacements of fluorapatite. The conversion from fluorapatite to pyromorphite is a common phenomenon in the supergene environment, resulting in an almost complete Pb → Ca and Cl → F substitution [50]. The formation of mimetite is considered to be related to the already mentioned As abundance in the Kihabe system. The described supergene mineralization is genetically related to post-Gondwana erosional episodes and the resulting supergene meteoric oxidation, spanning the period from the end of the Cretaceous to the Miocene (Figure 11; [51]).

Although not detected in the analyzed samples, the genesis of the vanadates at Kihabe can be associated with the same supergene processes that formed the Zn and Pb carbonates and phosphates (Figure 11). Vanadate deposits are widespread in the Otavi Mountainland [31], where they represent a special low-temperature, supergene-related, nonsulfide ore type [8]. The age of these vanadium ores appears to be generally confined to Cenozoic, with a distinct period of formation dated between 24 and 33 Ma [31]. The metallogenic history of V in the Aha Hills should not have been very different.

Finally, the occurrence of iodargyrite in the analyzed samples also has direct implications for the evolution of the supergene processes in the Aha Hills. In fact, the Ag-iodide is a common mineral in the supergene profiles of Au-Ag epithermal deposits occurring in arid to hyperarid areas [52], where it typically forms when the groundwaters are enriched in iodine, in response to extreme evaporation [52–55]. In the Kihabe case, the formation of iodargyrite could be related to the late stages of supergene alteration, which likely occurred during the transition from a humid to an arid climate, which has occurred since the Middle Miocene in several regions of southern Africa (Figure 11; [51,56]).

6. Conclusions

The Kihabe sulfide mineralization mainly consists of Fe-sphalerite and galena, finely disseminated in stratabound horizons within the quartzwacke, and shares several features with the ores of the Berg Aukas-type deposits (Namibia), suggesting a similar genesis. Among the nonsulfide assemblages, two mineralization types occur in the investigated samples: one characterized by hydrothermal willemite and baileychlore, and a second one instead consisting of supergene smithsonite, cerussite, Zn-Pb-phosphates, etc. Willemite is present in two generations, which should postdate sulfide emplacement, or form at their expenses. These characteristics are similar to those observed in the willemite occurrences of the Otavi Mountainland, which formed due to hydrothermal processes, during the final stages of the Damara Orogeny. The formation of the Kihabe willemite is likely coeval. Baileychlorite is characterized by textures indicating direct precipitation from solutions and dissolution–crystallization mechanisms. Both processes are typical of hydrothermal systems, thus suggesting the hydrothermal genesis of the Kihabe Zn-chlorite. Baileychlorite could represent an alteration halo possibly associated either with the sulfide or with willemite mineralization. The other nonsulfide minerals, smithsonite, cerussite and various Pb-phosphates, are clearly genetically associated with late phases of supergene alteration, which overprinted both the sulfide and the willemite- and baileychlore-bearing mineralizations. Supergene alteration probably occurred in this part of Botswana from the Late Cretaceous to the Miocene.

Author Contributions: Conceptualization, N.M. and M.B.; validation, N.M., G.B.; methodology and formal analysis, G.B., F.P., and L.S.; investigation, N.M., M.B., G.B.; data curation, N.M., G.B., N.F.; writing—original draft preparation, N.M., M.B.; writing—review and editing, N.M., M.B., G.B.; project administration, M.B.; funding acquisition, N.M., M.B. All authors have read and agreed to the published version of the manuscript.

Funding: The research leading to these results has received funding from the University of Naples Federico II (Italy) to M. Boni and N. Mondillo.

Acknowledgments: We would like to thank the Mt. Burgess personnel, very helpful in supplying geological information and other literature data. The authors at the University of Napoli wish to thank also R. de' Gennaro for the assistance during SEM analyses. We are grateful to G. Borg and three anonymous reviewers for comments and suggestions, which greatly enhanced the quality of the paper.

Conflicts of Interest: The authors declare no conflict of interest.

Appendix A

Table A1. Representative chemical compositions of willemite, smithsonite and cerussite (SEM-EDS).

Analyte	KDD 143-16	KDD 143-16	KDD 143-16	KDD 143-16	KDD 143-22	KDD 143-22	KDD 143-22	KDD 143-22	KDD 143-21	KDD 143-21	KDD 143-22	KDD 143-22	KDD 143-22	KDD 143-22	KDD 143-22
	Willemite	Willemite	Willemite	Willemite	Willemite	Willemite	Willemite	Willemite	Smithsonite	Smithsonite	Smithsonite	Smithsonite	Smithsonite	Cerussite	Cerussite
SiO ₂	25.55	26.17	25.77	26.11	26.91	26.35	26.90	26.04	n.a.	n.a.	n.a.	n.a.	n.a.	n.a.	n.a.
ZnO	70.91	70.68	68.65	72.38	71.88	71.46	69.93	71.31	62.72	61.83	62.88	60.07	63.34	2.70	1.82
FeO	0.12	0.22	0.88	0.04	0.18	0.78	0.06	0.36	0.23	0.34	0.04	2.77	0.22	0.16	b.d.
MnO	0.13	0.09	0.02	b.d.	0.16	b.d.	0.18	b.d.	b.d.	0.18	b.d.	b.d.	0.06	0.14	0.29
MgO	b.d.	0.15	b.d.	b.d.	0.11	0.07	0.19	0.28	0.28	0.33	b.d.	0.38	0.42	0.14	0.15
CaO	0.06	0.17	0.10	0.01	b.d.	b.d.	0.02	0.06	0.08	b.d.	0.06	0.06	0.24	0.55	0.41
CdO	0.14	0.42	b.d.	b.d.	0.08	b.d.	0.08	b.d.	0.25	b.d.	0.32	0.67	0.40	b.d.	b.d.
PbO	b.d.	0.03	0.16	0.18	b.d.	0.21	1.51	0.26	0.30	0.07	0.21	0.16	0.46	78.47	78.33
BaO	n.a.	n.a.	n.a.	n.a.	n.a.	n.a.	n.a.	n.a.	n.a.	n.a.	n.a.	n.a.	n.a.	0.24	0.15
As ₂ O ₅	2.87	2.18	2.43	1.91	1.35	1.90	0.52	2.02	0.58	0.78	0.72	0.13	0.29	b.d.	b.d.
CO ₂ *									34.85	34.50	34.57	34.97	35.42	17.78	17.14
Total	99.78	100.12	98.00	100.64	100.66	100.76	99.40	100.33	99.29	98.04	98.80	99.22	100.83	100.19	98.28

n.a., not analyzed; b.d., below detection limit; * CO₂ by stoichiometry.

Table A2. Chemical compositions (SEM-EDS) and structural formulae (in atoms per formula units, apfu) of baileychlore from the KDD 143 core. The number of cations are calculated on the basis of O₁₀(OH)₈.

Analyte	Rule and Radke (1988)	KDD 143-21	KDD 143-22	KDD 143-21	KDD 143-22	KDD 143-22	KDD 143-24	KDD143-24	KDD 143-26	KDD 143-26	KDD 143-26	KDD 143-26	KDD 143-26	KDD 143-26	KDD 143-26	KDD 143-26	KDD 143-26
		Site 5 Spectrum 3	Site 5 Spectrum 1	Site 7 Spectrum 3	Site 2 Spectrum 3	Site 3 Spectrum 2	Site 12 Spectrum 1	Site 12 Spectrum 2	Site 1 Spectrum 3	Site 4 Spectrum 8	Site 4 Spectrum 4	Site 7 Spectrum 1	Site 7 Spectrum 2	Site 5 Spectrum 2	Site 5 Spectrum 2	Site 10 Spectrum 4	Site 1 Spectrum 3
SiO ₂	32.00	28.48	29.09	30.00	31.41	31.30	29.68	29.88	30.74	30.48	29.52	30.28	27.55	31.32	30.91	26.68	26.06
TiO ₂		0.01		0.07	0.09	0.13	–	0.08	0.12	–	0.36	0.32	0.14	–	–	–	–
Al ₂ O ₃	12.40	10.97	11.55	10.27	12.91	12.89	11.35	11.66	15.31	15.15	14.14	16.05	13.84	14.19	15.42	13.57	14.24
FeO	12.90	0.51	0.65	0.15	0.31	1.10	1.29	1.60	1.62	1.01	0.87	1.15	0.79	1.36	1.76	1.64	0.79
MnO	0.15	–	0.11	0.04	–	0.17	0.25	0.14	0.12	0.04	0.18	0.13	–	0.03	–	0.06	–
MgO	4.60	1.84	1.95	1.69	2.09	1.68	2.14	2.32	1.96	1.90	1.70	2.44	3.57	1.76	2.09	2.19	1.52
CaO	1.00	0.35	0.42	0.64	0.57	0.64	0.65	0.59	0.45	0.51	0.55	0.42	0.38	0.58	0.31	0.36	0.27
ZnO	30.50	47.64	46.26	46.02	45.26	41.58	43.22	43.76	40.65	42.04	41.71	41.70	41.57	37.47	38.91	43.42	44.38
CuO	–	–	–	–	–	–	0.12	–	1.10	1.40	1.13	0.90	0.88	1.54	0.72	0.55	0.50
Total apfu	93.55	89.80	90.03	88.88	92.64	89.49	88.70	90.02	92.06	92.53	90.16	93.40	88.72	88.25	90.12	88.46	87.76
		tetrahedral cations (Σ = 4)															
Si	3.52	3.46	3.49	3.63	3.57	3.64	3.56	3.53	3.46	3.44	3.44	3.36	3.28	3.62	3.51	3.25	3.21
Al ^{IV}	0.48	0.54	0.51	0.37	0.43	0.36	0.44	0.47	0.54	0.56	0.56	0.64	0.72	0.38	0.49	0.75	0.79
Al ^{VI}	1.13	1.04	1.12	1.10	1.30	1.40	1.17	1.16	1.49	1.45	1.38	1.46	1.23	1.56	1.57	1.20	1.28
Ti	0.00	0.00	0.00	0.01	0.01	0.01	0.00	0.01	0.01	0.00	0.03	0.03	0.01	0.00	0.00	0.00	0.00
Fe ²⁺	1.19	0.05	0.07	0.02	0.03	0.11	0.13	0.16	0.15	0.10	0.08	0.11	0.08	0.13	0.17	0.17	0.08
Mn	0.01	0.00	0.01	0.00	0.00	0.02	0.03	0.01	0.01	0.00	0.02	0.01	0.00	0.00	0.01	0.01	0.00
Mg	0.75	0.33	0.35	0.30	0.35	0.29	0.38	0.41	0.33	0.32	0.29	0.40	0.63	0.30	0.35	0.40	0.28
Ca	0.12	0.05	0.05	0.08	0.07	0.08	0.08	0.08	0.05	0.06	0.07	0.05	0.05	0.07	0.04	0.05	0.04
Zn	2.48	4.28	4.10	4.11	3.80	3.57	3.83	3.82	3.38	3.50	3.59	3.42	3.66	3.20	3.26	3.91	4.04
Cu	0.00	0.00	0.00	0.00	0.00	0.00	0.12	0.00	1.10	1.40	1.13	0.90	0.88	1.54	0.72	0.55	0.50
Sum Oct.	5.68	5.75	5.70	5.62	5.56	5.48	5.74	5.65	6.52	6.83	6.59	6.38	6.54	6.80	6.11	6.29	6.22
R ²⁺	4.55	4.71	4.58	4.51	4.25	4.07	4.57	4.48	5.02	5.38	5.18	4.89	5.30	5.24	4.54	5.09	4.94

–, not detected.

Table A3. Representative chemical composition (SEM-EDS) of miscellaneous minerals detected in the Kihabe nonsulfide associations.

Analyte	KDD 143-24	KDD 143-24	KDD 143-24	KDD 143-26	KDD 143-26	KDD 143-26	KDD 143-26	KDD 143-26	KDD 143-22	KDD 143-22	KDD 143-22	KDD 143-22	KDD 143-22	KDD 143-22
	Mimetite	Mimetite	Mimetite	Pyromorphite	Pyromorphite	Hinsdalite	Hinsdalite	Hinsdalite	Fe-Oxy- hydroxides	Fe-Oxy- hydroxides	Fe-Oxy- hydroxides	Fe-Oxy- hydroxides	Fe-Oxy- hydroxides	Fe-Oxy- hydroxides
Al ₂ O ₃	n.a.	n.a.	n.a.	n.a.	n.a.	16.45	19.78	16.59	0.52	1.04	1.50	1.24	0.20	0.65
Fe ₂ O ₃	n.a.	n.a.	n.a.	n.a.	n.a.	5.64	1.28	4.20	95.98	91.49	91.30	87.22	81.00	74.52
ZnO	b.d.	0.50	b.d.	0.35	0.76	2.18	2.75	1.73	1.78	1.15	1.96	2.89	1.99	4.98
FeO	b.d.	b.d.	2.85	0.06	0.31	5.13	1.17	3.82	n.a.	n.a.	n.a.	n.a.	n.a.	n.a.
MnO	0.22	b.d.	b.d.	0.28	0.06	b.d.	b.d.	b.d.	b.d.	0.20	b.d.	b.d.	b.d.	0.01
MgO	b.d.	b.d.	b.d.	0.11	b.d.	b.d.	0.16	b.d.	b.d.	0.39	0.14	b.d.	0.05	0.11
CaO	0.03	0.35	0.31	2.08	1.15	0.63	0.22	0.13	0.05	b.d.	0.05	b.d.	0.25	0.19
CdO	0.32	0.24	0.03	b.d.	0.20	b.d.	b.d.	0.18	b.d.	0.29	0.13	0.86	b.d.	0.02
PbO	74.57	73.23	74.47	78.46	80.47	45.98	38.22	42.21	1.02	3.13	1.65	1.36	5.61	2.89
SrO	b.d.	b.d.	b.d.	0.92	0.81	0.35	0.38	0.28	b.d.	0.81	0.40	0.08	0.28	0.20
BaO	0.11	0.04	0.41	0.46	b.d.	0.74	0.18	b.d.	b.d.	0.15	0.12	0.25	b.d.	b.d.
As ₂ O ₅	22.08	21.22	21.95	b.d.	0.26	1.40	1.50	1.97	0.57	0.60	0.01	1.93	2.00	b.d.
P ₂ O ₅	0.44	0.53	0.27	16.19	15.27	11.38	10.04	9.35	n.a.	n.a.	n.a.	n.a.	n.a.	n.a.
Cl	2.46	2.62	3.32	2.93	2.91	0.50	0.10	0.38	n.a.	n.a.	n.a.	n.a.	n.a.	n.a.
SO ₃	n.a.	n.a.	n.a.	n.a.	n.a.	9.42	9.78	8.86	n.a.	n.a.	n.a.	n.a.	n.a.	n.a.
Total	100.23	98.73	103.63	101.83	102.18	99.78	85.54	89.70	99.92	98.43	97.26	95.83	91.38	83.56

n.a., not analyzed; b.d., below detection limit.

Table A4. Chemical analyses (wt. %) of selected Kihabe samples (ICP-ES-MS).

Analyte	Sample #	KDD 125-2	KDD 125-4	KDD 125-5	KDD 125-7	KDD 125-8	KDD 125-9	KDD 125-10	KDD 125-12	KDD 125-14	KDD 143-16	KDD 143-18	KDD 143-20	KDD 143-21	KDD 143-22	KDD 143-23	KDD 143-24	KDD 143-25	KDD 143-26	KDD 143-27	KDD 143-29	
wt. %	Det. Lim.																					
SiO ₂	0.01	81.03	76.58	76.6	79.17	77.47	80.65	81.44	82.05	82.15	81.97	74.09	79.8	75.41	76.63	67.85	72.35	75.59	76.26	83.27	78.04	
Ti	0.001	0.08	0.09	0.08	0.12	0.09	0.09	0.14	0.13	0.06	0.07	0.24	0.07	0.08	0.10	0.09	0.08	0.06	0.09	0.11	0.07	
Al	0.01	4.26	3.57	4.38	4.64	3.51	3.54	3.75	4.70	4.03	3.30	3.85	3.92	3.71	3.20	3.27	3.26	3.43	3.18	3.95	3.60	
Fe	0.01	0.76	1.07	2.20	0.62	0.84	0.72	1.38	1.11	0.51	0.61	0.92	0.59	0.69	0.76	0.82	0.96	0.66	0.64	0.57	0.47	
Mg	0.01	0.10	0.09	0.10	0.12	0.10	0.09	0.10	0.13	0.11	0.19	0.27	0.19	0.21	0.15	0.22	0.18	0.24	0.26	0.17	0.14	
Ca	0.01	0.02	0.02	0.01	0.02	0.02	0.02	0.02	0.01	b.d.	0.04	0.10	0.05	0.05	0.05	0.05	0.06	0.08	0.11	0.09	0.10	
Na	0.01	b.d.	0.03	0.03	0.03	0.03	0.03	0.03	0.03	0.03	0.02	b.d.	0.03	0.03	0.02	0.02	0.06	0.08	0.07	0.08	0.06	
K	0.01	2.30	2.07	2.37	2.54	2.03	2.14	2.13	2.67	2.55	1.86	2.33	2.29	2.15	1.83	1.81	1.75	2.09	1.61	2.54	1.86	
P	0.01	0.02	0.03	0.02	0.02	0.02	0.02	0.02	0.02	0.02	0.02	0.04	0.02	0.02	0.03	0.03	0.03	0.03	0.03	0.03	0.02	
S	0.05	0.44	2.42	1.71	0.07	1.45	1.78	1.80	0.06	b.d.	b.d.	b.d.	b.d.	b.d.	b.d.	b.d.	b.d.	b.d.	b.d.	b.d.	0.19	
Zn	0.0005	0.03	4.30	3.08	0.19	4.28	3.09	1.40	0.07	0.53	3.37	4.91	3.49	6.04	5.12	9.32	7.06	4.66	5.24	0.96	1.47	
Pb	0.0005	2.61	1.94	0.96	3.09	1.38	1.05	0.48	0.20	1.80	0.33	1.02	0.57	0.26	2.04	2.02	1.30	2.56	1.82	0.54	4.82	
mg/kg																						
Li	0.5	6.8	5.8	5.7	9.9	5.8	6.7	5.9	8	6.8	15.4	10.9	7.5	7.9	9.5	10.2	11	7.2	6.9	9.7	8.9	
V	10	21	19	24	31	23	15	20	29	16	16	51	18	58	262	23	27	19	20	28	20	
Cr	1	60	14	91	13	65	10	87	12	51	12	84	10	72	18	66	9	54	14	63	7	
Mn	5	39	58	45	42	51	44	40	34	33	45	45	42	42	46	47	52	39	35	38	40	
Co	1	b.d.	2	2	b.d.	4	5	7	b.d.	b.d.	2	9	8	10	8	25	18	32	31	5	3	
Ni	0.5	3	4.9	6.8	1.1	7.3	8.6	15.7	b.d.	2.8	3.8	21.1	10.9	13.3	8.9	20	11.3	12.6	12.3	7.5	2.1	
Cu	0.5	49.9	20.7	15.2	33.8	103.8	9.1	6.7	4.2	62.4	66.1	204.5	176.6	424.1	794.6	1831.5	1394.2	973.7	1131.5	477.1	1365.7	
As	5	294	256	182	406	419	29	41	64	134	275	76	72	81	117	3647	2007	172	119	39	42	
Rb	0.5	81.5	75.5	85.9	94.9	74	75.1	80.1	105.3	97.3	72.5	92.1	85.7	81.3	70.3	67.7	69.3	73.3	54.5	91.7	76.8	
Sr	5	46	10	7	8	7	5	6	7	20	5	8	10	7	13	7	6	31	28	13	28	
Y	0.5	2.5	2.9	2.8	4.3	25	8.7	10.3	11.6	6.5	5.9	9.7	6.7	6.3	6.6	6.2	6.3	6.6	6.8	7.2	6.9	
Zr	0.5	52.7	48.9	48.3	62.1	48.5	45.6	72.5	66.6	43.9	41.6	113.8	46.3	44.7	48.4	44.6	40	48.7	50.1	49.7	44.2	
Nb	0.5	3.5	3.1	3.1	4.5	3.1	3.8	5.2	4.5	3	3.3	8.9	3	3.4	3.9	3.1	3	2.3	3.6	4.2	3.1	
Mo	0.5	1.4	1.4	1.6	1.5	1.4	1.3	1.4	1.8	1.1	1.4	1	2.2	2.1	3.7	11.9	2.8	2	2.3	1.5	4.4	
Ag	0.5	50.3	38.8	20.7	99.8	39.3	12.1	7.8	27.2	27.7	17.6	49.2	15.9	17.8	47.3	39.8	39	103.1	112	27.7	102.8	
Cd	0.5	0.5	200.7	100.9	6.4	114.2	271.4	69.8	6.5	35	50.7	144.7	86.6	186.9	131.4	410.2	417.8	7.8	10.2	1.4	2177.5	
Sb	0.5	1.2	1.2	1.6	1.2	0.9	0.8	b.d.	1.2	0.5	3.6	2.6	1.5	4.2	9.1	28.3	24.6	5.7	5.7	2.6	12.2	
Ba	5	140	92	112	153	109	97	100	146	307	166	218	205	204	188	183	165	347	1232	253	957	
La	0.5	21.9	19.8	20.6	29.7	24.8	24.8	27.4	28.1	24.2	12.9	27.7	23.9	22	15.7	14.7	15.3	17.7	13.8	19.5	18.1	
Ce	5	43	39	41	61	49	48	56	53	47	27	54	46	42	29	29	29	36	28	37	35	
Hf	0.5	1.6	1.5	1.4	1.4	1.5	1.4	2.2	1.8	1.3	1.3	3.2	1.4	1.4	1.3	1.1	1	1.2	1.5	1.1	1	
Th	0.5	5.1	5.9	6.2	7.4	5.5	5.6	10.2	7.5	4.2	4.1	16.9	4.6	4.7	8.2	6.2	5.1	4.1	7	6.6	4.8	
U	0.5	2	3.2	2.7	5.5	4.7	1.3	1.7	1.8	1.9	0.8	1.9	1	1.1	1.8	2.6	2.1	1.6	1.3	1.2	1.3	

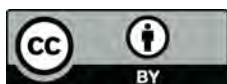
b.d., below detection limit.

References

1. Botswana Geoscience Institute. Botswana Mineral Projects and Prospects. Ministry of Mineral Resources, Green Technology and Energy Security. 2020, p. 28. Available online: <http://www.bgi.org.bw/sites/default/files/Brochure%20on%20Botswana%20Mineral%20Projects%20and%20Prospects%202020%20Version.pdf> (accessed on 1 July 2020).
2. Cairncross, B. The Otavi Mountain Land Cu-Pb-Zn-V Deposits. *Mineral. Rec.* **1997**, *28*, 109–130.
3. Melcher, F.; Oberthür, T.; Rammelmair, D. Geochemical and mineralogical distribution of germanium in the Khusib Springs Cu-Zn-Pb-Ag sulfide deposit, Otavi Mountain Land, Namibia. *Ore Geol. Rev.* **2006**, *28*, 32–56. [[CrossRef](#)]
4. Pirajno, F.; Joubert, B.D. An overview of carbonate-hosted mineral deposits in the Otavi mountain land, Namibia; implications for ore genesis. *J. Afr. Earth Sci.* **1993**, *16*, 265–272. [[CrossRef](#)]
5. Chetty, D.; Frimmel, H.E. The role of evaporites in the genesis of base metal sulphide mineralisation in the northern platform of the Pan-African Damara Belt, Namibia; geochemical and fluid inclusion evidence from carbonate wall rock alteration. *Mineral. Depos.* **2000**, *35*, 364–376. [[CrossRef](#)]
6. Hughes, M.J. The Tsumeb Ore Body, Namibia, and Related Dolostone-Hosted Base Metal Ore Deposits of Central Africa. Ph.D. Thesis, University of the Witwatersrand, Johannesburg, South Africa, 1987; p. 473.
7. Hitzman, M.W.; Reynolds, N.A.; Sangster, D.F.; Allen, C.R.; Carman, C.E. Classification, genesis, and exploration guides for nonsulfide Zinc deposits. *Econ. Geol.* **2003**, *98*, 685–714. [[CrossRef](#)]
8. Boni, M.; Mondillo, N. The “Calamines” and the “Others”: The great family of supergene nonsulfide zinc ores. *Ore Geol. Rev.* **2015**, *67*, 208–233. [[CrossRef](#)]
9. Melcher, F. The Otavi Mountain Land in Namibia: Tsumeb, Germanium and Snowball Earth. *Mitt. Österr. Miner. Ges.* **2003**, *148*, 413–435.
10. Mondillo, N.; Accardo, M.; Boni, M.; Boyce, A.; Herrington, R.; Rumsey, M.; Wilkinson, C. New insights into the genesis of willemite (Zn₂SiO₄) from zinc nonsulfide deposits, through trace elements and oxygen isotope geochemistry. *Ore Geol. Rev.* **2020**, *118*, 103307. [[CrossRef](#)]
11. Mount Burgess Mining N.L. Available online: <http://www.mountburgess.com> (accessed on 1 July 2020).
12. Carney, J.N.; Aldiss, D.T.; Lock, N.P. The geology of Botswana. *Botsw. Geol. S. Bull.* **1994**, *37*, 113.
13. Key, R.; Ayers, N. The 1998 Edition of the Geological Map of Botswana. *J. Afr. Earth Sci.* **2000**, *30*, 427–451. [[CrossRef](#)]
14. Lehmann, J.; Master, S.; Milani, L.; Kinnaird, J.A.; Naydenov, K.V.; Kumar, S.M. Regional aeromagnetic and stratigraphic correlations of the Kalahari Copperbelt in Namibia and Botswana. *Ore Geol. Rev.* **2015**, *71*, 169–190. [[CrossRef](#)]
15. Mapeo, R.B.M.; Wendorff, M.; Ramokate, L.V.; Armstrong, R.A.; Mphinyane, T.; Koobokile, M. Zircon geochronology of basement granitoid gneisses and sedimentary rocks of the Tsodilo Hills Group in the Pan-African Damara Belt, western Botswana: Age constraints, provenance, and tectonic significance. *J. Afr. Earth Sci.* **2019**, *159*, 103576. [[CrossRef](#)]
16. Meixner, H.M.; Peart, R.J. The Kalahari Drilling Project. *Botsw. Geol. S. Bull.* **1984**, *27*, 224.
17. Singletary, S.J.; Hanson, R.E.; Martin, M.W.; Crowley, J.L.; Bowring, S.A.; Key, R.M.; Ramokate, L.V.; Direng, B.B.; Krol, M.A. Geochronology of basement rocks in the Kalahari Desert, Botswana, and implications for regional Proterozoic tectonics. *Precambrian Res.* **2003**, *121*, 47–71. [[CrossRef](#)]
18. Wendorff, M. Outline of lithostratigraphy sedimentation and tectonics of the Tsodilo Hills Group, Neoproterozoic Lower Paleozoic siliciclastic succession in NW Botswana. *Ann. Soc. Geol. Pol.* **2005**, *75*, 17–25.
19. Killick, A.M. A preliminary account of the geology of the Kamtsas Formation of the Damara Sequence, eastern Gobabis District, South West Africa/Namibia. *Trans. Geol. Soc. S. Afr.* **1983**, *86*, 11–18.
20. Hoffman, K.H. New aspects of lithostratigraphic subdivision and correlation of Late Proterozoic to Early Cambrian rocks of the southern Damara Belt and their correlation with the central and northern Damara Belt and the Gariiep belt. *Namib. Geol. Surv. Commun.* **1989**, *5*, 59–67.
21. Schwartz, M.O.; Kwok, Y.Y.; Davis, D.W.; Akangyang, P. Geology, geochronology and regional correlation of the Ghanzi Ridge, Botswana. *S. Afr. J. Geol.* **1996**, *99*, 245–250.
22. Hanson, R.E. Proterozoic geochronology and tectonic evolution of southern Africa. *Geol. Soc. Lond. Spec. Publ.* **2003**, *206*, 427–463. [[CrossRef](#)]

23. Reeves, C.V. *Reconnaissance Aeromagnetic Survey of Botswana, 1975–1977*; Final interpretation report; Terra Surveys Ltd., Botswana Geological Survey: Lobatse, Botswana, 1978.
24. Chatupa, J.C.; Direng, B.B. Distribution of trace and major elements in the-180 + 75 μm and -75 μm fractions of the Sandveld regolith in northwest Ngamiland, Botswana. *J. Afr. Earth Sci.* **2000**, *30*, 515–534. [[CrossRef](#)]
25. Loxton, R.F. *A Photogeological Study of the Aha Hills, Northwest Botswana*; Loxton, Hunting and Associates, Report for Billiton Botswana (Pty) Ltd.: Gaborone, Botswana, 1981; p. 27.
26. Stalker, A.D. *Aha Hills Prospecting Licence 39180*; Final Report; Billiton Botswana (Pty) Limited: Gaborone, Botswana, 1983; p. 13.
27. Mapeo, R.B. *Geological and Structural Analysis of the Kihabe Base Metal Prospect in NW Botswana*; Internal Report for Mount Burgess (Botswana) (Pty) Ltd.: Gaborone, Botswana, 2007; p. 41.
28. Rule, A.C.; Radke, F. Baileychlore, the Zn end member of the trioctahedral chlorite series. *Am. Mineral.* **1988**, *73*, 135–139.
29. Gray, D.R.; Foster, D.A.; Goscombe, B.; Passchier, C.W.; Trouw, R.A.J. $^{40}\text{Ar}/^{39}\text{Ar}$ thermochronology of the Pan-African Damara Orogen, Namibia, with implications for tectonothermal and geodynamic evolution. *Prec. Res.* **2006**, *150*, 49–72. [[CrossRef](#)]
30. Schneider, J.; Boni, M.; Laukamp, C.; Bechstadt, T.; Petzel, V. Willemite (Zn_2SiO_4) as a possible Rb–Sr geochronometer for dating nonsulfide Zn–Pb mineralization: Examples from the Otavi Mountainland (Namibia). *Ore Geol. Rev.* **2008**, *33*, 152–167. [[CrossRef](#)]
31. Boni, M.; Terracciano, R.; Evans, N.; Laukamp, C.; Schneider, J.; Bechstadt, T. Genesis of vanadium ore in Otavi Mountainland, Namibia. *Econ. Geol.* **2007**, *102*, 441–469. [[CrossRef](#)]
32. Brugger, J.; McPhail, D.C.; Wallace, M.; Waters, J. Formation of Willemite in Hydrothermal Environments. *Econ. Geol.* **2003**, *98*, 819–835. [[CrossRef](#)]
33. Kamona, A.F.; Friedrich, G.H. Geology, mineralogy and stable isotope geochemistry of the Kabwe carbonate-hosted Pb–Zn deposit, Central Zambia. *Ore Geol. Rev.* **2007**, *30*, 217–243. [[CrossRef](#)]
34. Mondillo, N.; Herrington, R.; Boyce, A.J.; Wilkinson, C.; Santoro, L.; Rumsey, M. Critical elements in non-sulfide Zn deposits: A reanalysis of the Kabwe Zn–Pb ores (central Zambia). *Mineral. Mag.* **2018**, *82*, S89–S114. [[CrossRef](#)]
35. White, A.J.R.; Pearce, M.A.; Meadows, H.R. Distinguishing regional- and local-scale metasomatic systems at the Prairie Downs Zn–Pb deposit. *Lithos* **2016**, *262*, 247–265. [[CrossRef](#)]
36. Galley, A.G.; Hannington, M.D.; Jonasson, I.R. Mineral Deposits of Canada: A Synthesis of Major Deposit-Types, District Metallogeny, the Evolution of Geological Provinces, and Exploration Methods. In *Geological Association of Canada, Mineral Deposits Division, Special Publication No. 5*; Goodfellow, W.D., Ed.; Geological Association of Canada, Mineral Deposits Division: St. John’s, NL, Canada, 2007; pp. 141–161.
37. Spry, P.G.; Peter, J.M.; Slack, J.F. Meta-exhalites as exploration guides to ore. In *Metamorphosed and Metamorphogenic Ore Deposits*; Reviews in Economic Geology; Spry, P.G., Marshall, B., Vokes, F.M., Eds.; Society of Economic Geologists: Littleton, CO, USA, 2000; Volume 11, pp. 163–201.
38. Beaufort, D.; Rigault, C.; Billon, S.; Billault, V.; Inoue, A.; Inoue, S.; Patrier, P. Chlorite and chloritization processes through mixed-layer mineral series in lowtemperature geological systems—A review. *Clay Miner.* **2015**, *50*, 497–523. [[CrossRef](#)]
39. Abad, I.; Jimenez-Millan, J.; Sanchez-Roa, C.; Nieto, F.; Velilla, N. Neocrystallization of clay minerals in the Alhama de Murcia Fault (southeast Spain): Implications for fault mechanics. *Clay Miner.* **2019**, *54*, 1–13. [[CrossRef](#)]
40. Do Campo, M.; Bauluz, B.; Nieto, F.; Papa, C.; Hongn, F. SEM and TEM evidence of mixed-layer illite-smectite formed by dissolution crystallization processes in continental Paleogene sequences in northwestern Argentina. *Clay Miner.* **2016**, *51*, 723–740. [[CrossRef](#)]
41. Bourdelle, F.; Cathelineau, M. Low-temperature chlorite geothermometry: A graphical representation based on a T–R²⁺–Si diagram. *Eur. J. Mineral.* **2015**, *27*, 617–626. [[CrossRef](#)]
42. Pacey, A.; Wilkinson, J.J.; Cooke, D.R. Chlorite and epidote mineral chemistry in porphyry ore systems: A case study of the Northparkes District, New South Wales, Australia. *Econ. Geol.* **2020**, *115*, 701–727. [[CrossRef](#)]
43. Balassone, G.; Nieto, F.; Arfe, G.; Boni, M.; Mondillo, N. Zn-clay minerals in the Skorpion Zn nonsulfide deposit (Namibia): Identification and genetic clues revealed by HRTEM and AEM study. *Appl. Clay Sci.* **2017**, *150*, 309–322. [[CrossRef](#)]

44. Mondillo, N.; Nieto, F.; Balassone, G. Micro and nano-characterization of Zn-clays in nonsulfide supergene ores of southern Peru. *Am. Mineral.* **2015**, *100*, 2484–2496. [[CrossRef](#)]
45. Choulet, F.; Charles, N.; Barbanson, L.; Branquet, Y.; Sizaret, S.; Ennaciri, A.; Badra, L.; Chen, Y. Non-sulfide zinc deposits of the moroccan high atlas: Multi-scale characterization and origin. *Ore Geol. Rev.* **2014**, *56*, 115–140. [[CrossRef](#)]
46. Choulet, F.; Richard, J.; Boiron, M.-C.; Dekoninck, A.; Yans, J. Distribution of trace elements in willemite from the Belgium non-sulphide deposits. *Eur. J. Mineral.* **2019**, *31*, 983–997. [[CrossRef](#)]
47. Coppola, V.; Boni, M.; Gilg, H.A.; Balassone, G.; Dejonghe, L. The “calamine” nonsulfide Zn–Pb deposits of Belgium: Petrographical, mineralogical and geochemical characterization. *Ore Geol. Rev.* **2008**, *33*, 187–210. [[CrossRef](#)]
48. Monteiro, L.V.S.; Bettencourt, J.S.; Juliani, C.; de Oliveira, T.F. Geology, petrography, and mineral chemistry of the Vazante non-sulfide and Ambrósia and Fagundes sulfide-rich carbonate-hosted Zn-(Pb) deposits, Minas Gerais. Brazil. *Ore Geol. Rev.* **2006**, *28*, 201–234. [[CrossRef](#)]
49. Gilg, H.A.; Boni, M.; Hochleitner, R.; Struck, U. Stable isotope geochemistry of carbonate minerals in supergene oxidation zones of Zn-Pb deposits. *Ore Geol. Rev.* **2008**, *33*, 117–133. [[CrossRef](#)]
50. Markl, G.; Marks, M.A.W.; Holzäpfel, J.; Wenzel, T. Major, minor, and trace element composition of pyromorphite-group minerals as recorder of supergene weathering processes from the Schwarzwald mining district, SW Germany. *Am. Mineral.* **2014**, *99*, 1133–1146. [[CrossRef](#)]
51. Partridge, T.C.; Maud, R.R. Geomorphic evolution of southern Africa since the Mesozoic. *S. Afr. J. Geol.* **1987**, *90*, 179–208.
52. Sillitoe, R.H. Supergene silver enrichment reassessed. In *Supergene environments, processes, and products. Soc. Econ. Geol. Spec. Publ.* **2009**, *14*, 15–32.
53. Boyle, D.R. Iodargyrite as an indicator of arid climatic conditions and its association with gold-bearing glacial tills of the Chibougamau-Chapais area, Quebec. *Can. Mineral.* **1997**, *35*, 23–34.
54. Gammons, C.H.; Yu, Y. The stability of aqueous silver bromide and iodine complexes at 25–300 °C. Experiments, theory and geologic applications. *Chem. Geol.* **1997**, *137*, 155–173. [[CrossRef](#)]
55. Golebiowska, B.; Pieczka, A.; Rzepa, G.; Matyszkiewicz, J.; Krajewski, M. Iodargyrite from Zalas (Cracow area, Poland) as an indicator of Oligocene–Miocene aridity in Central Europe. *Palaeogeogr. Palaeoclimatol. Palaeoecol.* **2010**, *296*, 130–137. [[CrossRef](#)]
56. Van der Wateren, F.M.; Dunai, T.G. Late Neogene passive margin denudation history—Cosmogenic isotope measurements from the central Namib desert. *Glob. Planet. Chang.* **2001**, *30*, 271–307. [[CrossRef](#)]



© 2020 by the authors. Licensee MDPI, Basel, Switzerland. This article is an open access article distributed under the terms and conditions of the Creative Commons Attribution (CC BY) license (<http://creativecommons.org/licenses/by/4.0/>).

The following extract from the JORC Code 2012 Table 1 is provided for compliance with the Code requirements for the reporting of drilling results.

Section 1 Sampling Techniques and Data (Criteria in this section apply to all succeeding sections).

Criteria	JORC code explanation	Commentary
Sampling techniques	<p>Nature and quality of sampling (eg cut channels, random chips, or specific specialised industry standard measurement tools appropriate to the minerals under investigation, such as down hole gamma sondes, or handheld XRF instruments, etc). These examples should not be taken as limiting the broad meaning of sampling. • Include reference to measures taken to ensure sample representivity and the appropriate calibration of any measurement tools or systems used. • Aspects of the determination of mineralisation that are Material to the Public Report. • In cases where 'industry standard' work has been done this would be relatively simple (eg 'reverse circulation drilling was used to obtain 1 m samples from which 3 kg was pulverised to produce a 30 g charge for fire assay'). In other cases more explanation may be required, such as where there is coarse gold that has inherent sampling problems. Unusual commodities or mineralisation types (eg submarine nodules) may warrant disclosure of detailed information.</p>	<p>Mount Burgess Mining Diamond Core Holes</p> <p>HQ Diamond Core was marked and collected in sample trays, visually logged and cut in half. Samples were collected as nominal 1m intervals but based on visible geology with minimum samples of 0.3m and maximum samples of 1.3m. Half of each core was retained on site in core trays and the other half was double bagged and sent to Intertek Genalysis Randburg, South Africa where they were crushed. A portion of each intersection sample was then pulverised to p80 75um and sent to Intertek Genalysis for assaying via ICPMS/OES for Ag/Co/Cu/Ga/Ge/In/Pb/V/Zn.</p> <p>Mount Burgess Mining Reverse Circulation Hole</p> <p>Individual meters of RC drill chips were bagged from the cyclone. These were then riffle split for storage in smaller bags, with selected drill chips being stored in drill chip trays. A trowel was used to select drill chip samples from sample bags to be packaged and sent to Intertek Genalysis, Randburg, South Africa where they were crushed. A portion of each intersection's sample was then pulverised to P80 75um and sent to Intertek Genalysis, Maddington, WA, for assaying via ICP/OES for Ag/Co/Cu/Pb/Zn.</p> <p>Mount Burgess Mining Diamond Core Samples submitted to for Metallurgical Test Work</p> <p>The remainder of the crushed samples were then sent from Intertek Genalysis Randburg to Intertek Genalysis Maddington, Western Australia where they were then collected by the Company for storage. Samples from various intersections from six drill holes NXDD030, NXDD033, NXDD037, NXDD039, NXDD040 and NXDD043, as shown in Figure 1 of the Company's announcement of 28 May 2019 to ASX, were selected by the Company for submission to for sensor sorter metallurgical test work. These samples were chosen to determine if Sighter Test Work developed by STEINERT could be used to pre-concentrate zinc, lead, silver, germanium and vanadium pentoxide mineralization prior to milling and flotation. Results of the +4mm STEINERT Metallurgical Test Work were reported on 20 August 2019.</p>

	Drill type (eg core, reverse circulation, open-hole hammer, rotary air blast, auger, Bangka, sonic, etc) and details (eg core diameter, triple or standard tube, depth of diamond tails, face-sampling bit or other type, whether core is oriented and if so, by what method, etc).	<p>Mount Burgess Mining Diamond Core Holes</p> <p>HQ diameter triple tube was used for diamond core drilling. As all holes drilled into the Nxuu deposit were vertical holes the diamond core was not orientated.</p> <p>Mount Burgess Mining RC Hole</p> <p>One vertical RC hole was drilled into the Nxuu Deposit mineralised zone.</p>
Drill sample recovery	Method of recording and assessing core and chip sample recoveries and results assessed. • Measures taken to maximise sample recovery and ensure representative nature of the samples. • Whether a relationship exists between sample recovery and grade and whether sample bias may have occurred due to preferential loss/gain of fine/coarse material	<p>Mount Burgess Mining Diamond Core and RC Holes</p> <p>Sample recoveries were in general high and no unusual measures were taken to maximise sample recovery other than the use of triple tube core for diamond core drilling. Mount Burgess believes there is no evidence of sample bias due to preferential loss/gain of fine/coarse material.</p>
Logging	Whether core and chip samples have been geologically and geotechnically logged to a level of detail to support appropriate Mineral Resource estimation, mining studies and metallurgical studies. • Whether logging is qualitative or quantitative in nature. Core (or costean, channel, etc) photography. • The total length and percentage of the relevant intersections logged.	<p>Mount Burgess Mining Diamond Core Holes and RC Hole</p> <p>Holes were logged in the field by qualified Geologists on the Company's log sheet template and of sufficient detail to support future mineral resource estimation: Qualitative observations covered Lithology, grain size, colour, alteration, mineralisation, structure. Quantitative logging included vein percent. SG calculations at ~5m intervals were taken in the DD holes. All holes were logged for the entire length of hole. Logs are entered into MTBs GIS database managed by MTB in Perth.</p>
Sub-sampling techniques and sample preparation	If core, whether cut or sawn and whether quarter, half or all core taken. • If non-core, whether riffled, tube sampled, rotary split, etc and whether sampled wet or dry. • For all sample types, the nature, quality and appropriateness of the sample preparation technique. • Quality control procedures adopted for all sub-sampling stages to maximise representivity of samples. • Measures taken to ensure that the sampling is representative of the in situ material collected, including for instance results for field duplicate/second-half sampling. • Whether sample sizes are appropriate to the grain size of the material being sampled	<p>Mount Burgess Mining Diamond Holes and RC Hole</p> <p>HQ Core was sawn in half on site. Half of each core was retained on site in core trays and the other half was double bagged and labelled noting Hole# and interval both within the bag and on the bag. Sample bags were then placed in larger bags of ~40 individual samples and the larger bag also labelled describing the contents. Field duplicates were inserted at regular intervals.</p> <p>All samples currently being reported on were assayed for Ag/Co/Cu/Ga/Ge/In/Pb/V/Zn.</p> <p>All RC sample bags were labelled with drill hole number and sample interval and collectively stored in larger bags with similar reference. Drill chip trays were all stored separately.</p> <p>All samples currently reported on were assayed for Ag/Co/Cu/Pg/Zn.</p>

<p>Quality of assay data and laboratory tests</p>	<ul style="list-style-type: none"> •The nature, quality and appropriateness of the assaying and laboratory procedures used and whether the technique is considered partial or total •For geophysical tools, spectrometers, hand-held XRF instruments, etc, the parameters used in determining the analysis including instrument make and model, reading times, calibration factors applied and their derivation etc. • nature of quality control procedures adopted (e.g. standards, blanks, duplicates, external laboratory checks) and whether acceptable levels of accuracy (i.e. lack of bias) and precision have been established. 	<p>All Mount Burgess Samples</p> <p>All samples, when originally assayed, were sent to Intertek Genalysis Perth, for assaying according to the following standard techniques:</p> <p>Diamond Core Samples</p> <ul style="list-style-type: none"> (a) Ore grade digest followed by ICP – OES finish for Silver, Lead, Vanadium & Zinc (b) Nitric acid/hydrofluoric acid specific digest for Germanium and Indium (c) Also 4 acid digest for silver, lead, zinc, germanium and gallium followed by AAS <p>RC Samples</p> <p>Ore grade digest followed by ICP-OES for Ag/Co/Cu/Pb/Zn</p> <p>All samples submitted for the Steinert Test Work, once separated through the Sensor Sorter process, were then submitted to NAGROM Laboratories for the upgraded concentrates to then be assayed by mixed acid digest with ICP finish for Vanadium, Lead, Zinc and Silver.</p> <p>Mount Burgess quality control procedures include following standard procedures when sampling, including sampling on geological intervals, and reviews of sampling techniques in the field.</p> <p>The current laboratory procedures applied to the Mount Burgess sample preparation include the use of cleaning lab equip. w/ compressed air between samples, quartz flushes between high grade samples, insertion of crusher duplicate QAQC samples, periodic pulverised sample particle size (QAQC) testing and insertion of laboratory pulp duplicates QAQC samples according to Intertek protocols.</p> <p>Intertek inserts QA/QC samples (duplicates, blanks and standards) into the sample series at a rate of approx. 1 in 20. These are tracked and reported on by Mount Burgess for each batch. When issues are noted the laboratory is informed and investigation conducted defining the nature of the discrepancy and whether further check assays are required. The laboratory completes its own QA/QC procedures and these are also tracked and reported on by Mount Burgess. Acceptable overall levels of analytical precision and accuracy are evident from analyses of the routine QAQC data</p>
<p>Verification of sampling and assaying</p>	<p>The verification of significant intersections by either independent or alternative company personnel. • The use of twinned holes. • Documentation of primary data, data entry procedures, data verification, data storage (physical and electronic) protocols. • Discuss any adjustment to assay data.</p>	<p>All Mount Burgess Samples</p> <p>Assay results for samples were received electronically from Intertek Genalysis and uploaded into MTB's database managed by MTB at its Perth Office.</p> <p>Analytical results for Vanadium (V) from diamond core holes being reported on have now been converted to V2O5 (Vanadium Pentoxide) by multiplying the Vanadium grades by 1.785.</p>
<p>Location of data points</p>	<p>Accuracy and quality of surveys used to locate drill holes (collar and down-hole surveys), trenches, mine workings and other locations used in Mineral Resource estimation. • Specification of the grid system used. • Quality and adequacy of topographic control.</p>	<p>All Mount Burgess Holes</p> <p>Drill hole collar locations were recorded at the completion of each hole by hand held Garmin 62S GPS with horizontal accuracy of approx. 5 metres • Positional data was recorded in projection WGS84 UTM Zone 34S. The accuracy provided by the system employed is sufficient for the nature of the exploratory program. Downhole surveys were not conducted.</p>
<p>Data spacing and distribution</p>	<p>Data spacing for reporting of Exploration Results. • Whether the data spacing and distribution is sufficient to establish the degree of geological and grade continuity appropriate for the Mineral Resource and Ore Reserve estimation procedure(s) and classifications applied. • Whether sample compositing has been applied.</p>	<p>All Mount Burgess Holes</p> <p>Mount Burgess drilling campaigns were undertaken to validate historical drilling as well as to acquire further data for future resource estimation.. The data spacing and distribution is currently insufficient to establish the degree of geological and grade continuity appropriate for the estimation of Mineral Resources compliant with the 2012 JORC Code.</p> <p>Additional drilling is planned to determine the extent of mineralisation and estimate a Mineral Resource</p>

		compliant with the 2012 JORC Code. Sample compositing was conducted on four Nxuu deposit drill holes, following receipt of assays from Intertek Genalysis, for the purpose of mineralogical and metallurgical test work.
Orientation of data in relation to geological structure	Whether the orientation of sampling achieves unbiased sampling of possible structures and the extent to which this is known, considering the deposit type. • If the relationship between the drilling orientation and the orientation of key mineralised structures is considered to have introduced a sampling bias, this should be assessed and reported if material.	All Mount Burgess Holes Mineralisation was typically intersected at -90 degrees at the Nxuu Deposit and the Company believes that unbiased sampling was achieved.
Sample security	The measures taken to ensure sample security.	All Mount Burgess Holes Samples were taken by vehicle on the day of collection to MTB's permanent field camp, and stored there until transported by MTB personnel to Maun from where they were transported via regular courier service to laboratories in South Africa.
Audits or reviews	The results of any audits or reviews of sampling techniques and data.	All Mount Burgess Diamond Core Holes An independent Geologist was engaged to review sampling and logging methods on site at the commencement of the program. Mount Burgess RC Hole MTB's Exploration Manager continually reviewed sampling and logging methods on site at the commencement of all programs.

Section 2 Reporting of Exploration Results (Criteria listed in the preceding section also apply to this section).

Criteria	JORC Code Explanation	Commentary
Mineral tenement and land tenure status	Type, reference name/number, location and ownership including agreements or material issues with third parties such as joint ventures, partnerships, overriding royalties, native title interests, historical sites, wilderness or national park and environmental settings.	The Kihabe-Nxuu Project is located in north-western Botswana, adjacent to the border with Namibia. The Project is made up of one granted prospecting licence - PL 43/2016, which covers an area of 1000 sq km. This licence is 100% owned and operated by Mount Burgess. The title is current at the time of release of this report, with a renewal granted to 31 December 2020 with a right to apply for a further two year renewal to 31 December 2022. PL 43/2016 is in an area designated as Communal Grazing Area.
	The security of the tenure held at the time of reporting along with any known impediments to obtaining a licence to operate in the area.	The licence is in good standing and no impediments to operating are currently known to exist.
Exploration done by other parties	Acknowledgment and appraisal of exploration by other parties.	The Geological Survey of Botswana undertook a program of soil geochemical sampling in 1982. As a result of this program, Billiton was invited to undertake exploration and drilling activities in and around the project area. Mount Burgess first took ownership of the project in 2003 and has undertaken exploration activities on a continual basis since then.
Geology	Deposit type, geological setting and style of mineralisation.	The Kihabe-Nxuu Project lies in the NW part of Botswana at the southern margin of the Congo craton. The Gossan Anomaly is centred on an exposed gossan within the project. To the north of the project are granitoids, ironstones, quartzites and mica schists of the Tsodilo Hills Group covered by extensive recent Cainozoic sediments of the Kalahari Group. Below the extensive Kalahari sediments are siliciclastic sediments and igneous rocks of the Karoo Supergroup in fault bounded blocks.
Drill hole Information	A summary of all information material to the understanding of the exploration results including a tabulation of the following information for all Material drill holes: eastings and northing of the drill hole collar elevation or RL (Reduced Level – elevation above sea level in metres) of the drill hole collar dip and azimuth of the hole down hole length and interception depth hole length If the exclusion of this information is justified on the basis that the information is not	Information material to the understanding of the exploration results reported by Mount Burgess is provided in the text of the public announcements released to the ASX. No material information has been excluded from the announcements.

Criteria	JORC Code Explanation	Commentary
	Material and this exclusion does not detract from the understanding of the report, the Competent Person should clearly explain why this is the case.	
Data aggregation methods	<p>In reporting Exploration Results, weighting averaging techniques, maximum and/or minimum grade truncations (eg cutting of high grades) and cut-off grades are usually Material and should be stated.</p> <p>Where aggregate intercepts incorporate short lengths of high grade results and longer lengths of low grade results, the procedure used for such aggregation should be stated and some typical examples of such aggregations should be shown in detail.</p> <p>The assumptions used for any reporting of metal equivalent values should be clearly stated.</p>	<p>All Mount Burgess Holes</p> <p>No data aggregation methods have been used. Vanadium results are reported without a top cut but the Company has used 100 ppm as a bottom cut.</p> <p>Vanadium Pentoxide results are reported by multiplying the Vanadium results by 1.785.</p>
Relationship between mineralisation widths and intercept lengths	<p>These relationships are particularly important in the reporting of Exploration Results.</p> <p>If the geometry of the mineralisation with respect to the drill hole angle is known, its nature should be reported.</p> <p>If it is not known and only the down hole lengths are reported, there should be a clear statement to this effect (eg 'down hole length, true width not known').</p>	<p>All Mount Burgess Holes</p> <p>The geometry of the mineralisation with respect to the drill hole angle is typically at -90 degrees at the Nxuu Deposit which is considered representative from a geological modelling perspective.</p>
Diagrams	Appropriate maps and sections (with scales) and tabulations of intercepts should be included for any significant discovery being reported These should include, but not be limited to a plan view of drill hole collar locations and appropriate sectional views.	<p>Billiton Percussion Holes pre-fixed AP</p> <p>The Company has no available information for these holes other than collar and survey data and assay results</p> <p>All Mount Burgess Holes</p> <p>Appropriate maps, sections and mineralised drill intersection details are provided in public announcements released to the ASX. Refer to the Company's website www.mountburgess.com.</p>
Balanced reporting	Where comprehensive reporting of all Exploration Results is not practicable, representative reporting of both low and high grades and/or widths should be practiced to avoid misleading reporting of Exploration Results.	Exploration results reported in Mount Burgess public announcements and this report are comprehensively reported in a balanced manner.
Other Substantive Exploration Data	Other exploration data, if meaningful and material, should be reported including (but not limited to): geological observations,	

Criteria	JORC Code Explanation	Commentary
	geophysical survey results, geochemical survey results, bulk samples – size and method of treatment, metallurgical test results, bulk density, ground water, geotechnical and rock characteristics, potential deleterious or contaminating substances.	
Further work	<p>The nature and scale of planned further work (eg tests for lateral extensions or depth extensions or large-scale step-out drilling).</p> <p>Diagrams clearly highlighting the areas of possible extensions, including the main geological interpretations and future drilling areas, provided this information is not commercially sensitive.</p>	<p>Further works planned at the Project include additional drilling and surface mapping at the Kihabe-Nxuu Zinc/Lead/Silver/Germanium and Vanadium Project.</p> <p>Further metallurgical test work will be conducted, including bulk testing to be conducted by STEINERT on the sensor sorter process. Bulk test work will also be conducted on the multishaft vertical milling process.</p>

ACN: 009 067 476
8/800 Albany Hwy, East Victoria Park,
Western Australia 6101
Tel: (61 8) 9355 0123
Fax: (61 8) 9355 1484
mtb@mountburgess.com
www.mountburgess.com